creative commons
COMMONS DEED

저작자표시-비영리-변경금지 2.0 대한민국

이용자는 아래의 조건을 따르는 경우에 한하여 자유롭게

- 이 저작물을 복제, 배포, 전송, 전시, 공연 및 방송할 수 있습니다.

다음과 같은 조건을 따라야 합니다:

저작자표시. 귀하는 원저작자를 표시하여야 합니다.

비영리. 귀하는 이 저작물을 영리 목적으로 이용할 수 없습니다.

변경금지. 귀하는 이 저작물을 개작, 변형 또는 가공할 수 없습니다.

- 귀하는, 이 저작물의 재이용이나 배포의 경우, 이 저작물에 적용된 이용허락조건을 명확하게 나타내어야 합니다.
- 저작권자로부터 별도의 허가를 받으면 이러한 조건들은 적용되지 않습니다.

저작권법에 따른 이용자의 권리는 위의 내용에 의하여 영향을 받지 않습니다.

이것은 이용허락규약(Legal Code)을 이해하기 쉽게 요약한 것입니다.

Disclaimer

dCollection

공학박사학위논문

개인 편차에 대해 정규화되고 설명 가능한 인공지능 기반 중심혈압파형 추론 및 심혈관계 질환 진단 방법 연구

Inference of Central Blood Pressure Waveform and Arterial Disease Diagnosis Using Explainable Artificial Intelligence Regularized for Individuality

2022 년 2 월

서울대학교 대학원

기계공학부

김 수 호

개인 편차에 대해 정규화되고 설명 가능한 인공지능 기반 중심혈압파형 추론 및 심혈관계 질환 진단 방법 연구

Inference of Central Blood Pressure Waveform and Arterial Disease Diagnosis Using Explainable Artificial Intelligence Regularized for Individuality

지도교수 윤 병 동

이 논문을 공학박사 학위논문으로 제출함

2021 년 10 월

서울대학교 대학원

기계공학부

김 수 호

김수호의 공학박사 학위논문을 인준함

2021 년 12 월

위 원 장 : 김 윤 영 (인)

부위원장 : 윤 병 동 (인)

위 원 : 김 도 년 (인)

위 원 : 신 용 대 (인)

위 원 : 한 진 오 (인)

Abstract

Inference of Central Blood Pressure Waveform and Arterial Disease Diagnosis Using Explainable Artificial Intelligence Regularized for Individuality

Sooho Kim
Department of Mechanical and Aerospace Engineering
The Graduate School
Seoul National University

Arterial diseases, such as peripheral artery occlusive disease (PAD), aorta aneurysm, arterial stiffening, and etc., are leading causes of death in the world. Arterial diseases are a highly prevalent entailing high morbidity and mortality risks and become projected to sharply increase with societal aging. In clinical practice today, arterial diseases diagnosis necessitates angiography techniques. These techniques are not ideally suited to affordable and convenient for arterial disease detection and severity assessment.

The analysis of arterial pulse waveforms (PWA) may play a complementary role to machine learning (ML) in PAD diagnosis. Indeed, PAD alters the morphology of

arterial pulse wave signals (BPW) by affecting the pulse wave propagation and reflection characteristics in the arteries. Hence, PWA has the potential to outperform techniques built upon discrete fiducial points in the arterial pulse wave signals by allowing the exploitation of the arterial pulse wave signals in their entirety. Also, PWA may be combined with modern deep learning (DL) to leverage its ability for automatic feature selection. Meanwhile, A clinical approaches more focus on PWA with arterial pulse wave signals measured at the central locations. These central pulse waveforms such as central blood pressure waveforms, are contains rich information about dynamic cardiovascular status.

For in real applications, there are obvious challenges in incorporintg DL into PWA. First, the dataset is limited: naïve application of DL to PWA-based PAD diagnosis requires massive longitudinal datasets associated with PAD progression in time, which preferably also encompass diverse anatomical and physiological characteristics as well as disease severity levels. In real, (1) the dataset from the patients under scarce disease severity levels deteriorates the diagnosis and severity assessment performance of deep neural network (DNN) especially for the dataset which is under the severity levels unseen to DNN during training phase. Also, (2) the limited dataset related with limited anatomical and physiological characteristics may pose formidable challenges in training a DNN for PAD diagnosis which is generalizable to a wide range of anatomical and physiological characteristics. For central BPW analysis, (3) the excessive cost is required to measure the central BPW since it is commonly measured with the catheterization which is invasive measurement. To overcome theses obstacles, this doctoral dissertation aims at advancing three essential and co-related research areas: (1) Research Thrust 1 – A mutualy-informed neural network for severity assessment of

arterial disease to overcome the sparsity of disease severity levels given in training; (2) Research Thrust 2 – A continuous-propoerty adversrail regularization for individuality independency to overcome the sparsity of anatomical and physiological characteristics beynd the training dataset; (3) Research Thrust 3 – A sequence-oriented neural network for inference of central BPW to gather the central BPW accurately with non-expensive way.

Research Thrust 1: An initial proof-of-cencept of deep learning-based arterial pulse waveform analysis is proposed for affordable and convenient arterial disease screening as well as presents challenges that must be addressed for real-world clinical applications. As a preliminary study, the PAD diagnosis problem is investigated, and a deep convolutional neural network capable of detecting and assessing the severity of PAD based on the analysis of brachial and ankle arterial pulse waveforms is constructed, evaluated, and compared with the state-of-the-art ankle-brachial index (ABI) using the virtual patients. To investigate the efficacy of the DNN implementation, the visualization and latent feature space analysis of DNN is conducted. Furthermore, a method to training DNN-based diagnosis model with dataset under sparse PAD severity is proposed using mutualy information. The generative model is designed to compensate the sparse dataset, and the generative model and the diagnosis model are trained simultaneously and adversarily. The mutual information among latent code, which is an input of the generative model, generated data, and disease severity of known dataset is maximized to generate the data under desired disease severity level and finally maximize the performance of the diagnosis model.

Research Thrust 2: A continuous property-adversarial regularization (CPAR) approach is proposed to robust generalization of a DNN against scarce anatomical and

physiological characteristics of datasets. Inspired by domain-adversarial learning, the conventional discrete domain-adversarial regularization to enable regularization and generalization of a DNN across multiple continuous properties by reformulating the anti-domain classification formalism used in discrete domain-adversarial regularization to a novel anti-property regression formalism applicable to multiple continuous properties. The variation of continuous anatomical and physiological characteristics is discretized and defined as dispersed different domains, and all domain-adversrial learning is conducted. In this way, the proposed approach fosters the exploitation of latent features that can facilitate the intended task independently of confounding property-induced disturbances, by regularizing the extraction of disturbance-dependent latent features in the network's feature extraction layer.

Research Thrust 3: A sequence-oriented neural network is proposed to robust inference of central BPW by modulating distal BPWs. Inspired by Wavenet, which is applied for modulation of waveform data surprisingly decrease computational cost by utilizing convolutional neural network (CNN) architecture, conserving sequential characteristics. The conventional central BPW inference is conducted with hemodynamic model and its transfer function (TF), which shows low inference accuracy. The sequence-oriented neural network is composed of two sub-networks; CNN and RNN (recurrent neural network) based subnet. The specialized layers in CNN based subnet, single-sided layer, masked layer, and bottle-neck layer, are proposed for sequence-oriented computation. The processed data is finally modulated in RNN based subnet. In this way the proposed approach fosters the exact central BPW inference by causal and computationally feasible way.

Keywords: Arterial disease diagnosis
Peripheral arterial disease (PAD)
Pulse waveform analysis
Blood pressure waveform
Deep learning

Student Number: 2017-28145

Table of Contents

List of Tables

List of Figures

Nomenclatures

PAD	Peripheral arterial disease
PWA	Analysis of arterial pulse waveforms
ML	Machine learning
BPW	Blood pressure waveform
DL	Deep learning
DNN	Deep neural network
ABI	Ankle-brachial index
CPAR	Continuous-property adversarial regularization
TF	Transfer function
CNN	Convolutional neural network
RNN	Recurrent neural network
CVD	Cardiovascular disease
CV	Cardiovascular
TL	Transmission line
BP	Blood pressure
BF	Blood flow
t-SNE	t-distributed stochastic neighbor embedding
GradCAM	Gradient-weighted class activation
ROC	Receiver operating characteristic
AUC	Area under curve
GAN	Generative adversarial network
BA	Bland-Altman
IIV	Inter-individual variability
RMSE	Root mesn squared error

PWV	Pulse wave velocity
GTF	Generalized transfer function
ITF	Individualized transfer function
p_I	Inlet blood pressure wave
p_O	Outlet blood pressure wave
q_I	Inlet blood pressure flow
q_O	Outlet blood pressure flow
γ	Propagation constant
Γ	Reflection constant
l	Arterial length
Z_I	Input impedance
Z_C	Characteristic impedance
ρ	Blood density
σ	Poisson's ratio
ϕ	Phase difference
c_0	Pulse wave velocity
E	Young's modulus
h	Arterial wall thickness
D	Internal diameter
$D(x)$	Discriminator
$G(z)$	Generator
c_g	Latent code
$I(\mathrm{A}; B)$	Mutual information between A and B
$Q(\cdot)$	Auxiliary distribution
$\lambda_g, \lambda_s, \lambda_c$	hyperparameters
s_x	PAD severity

$G_f(\cdot)$	Feature extraction layer
$G_l(\cdot)$	Label prediction layer
$G_\eta(\cdot)$	Domain regression layer
$d_{\mathcal{H}}^{eff}$	Effective $\mathcal{H}$-idvergence

Chapter 1

Introduction

1.1 Motivation

Arterial diseases, such as peripheral artery occlusive disease (PAD), aorta aneurysm, arterial stiffening, and etc., are leading causes of death in the world. For examples, PAD is a highly prevalent vascular disease entailing high morbidity and mortality risks. The United States and the world are estimated to have >8 million (2000 [1]) and >200 million (in 2010 [2, 3]) patients with PAD. In addition, PAD may become even more prevalent and projected to sharply increase with societal aging. It makes a significant adverse impact on morbidity and quality of life, and also carries significant mortality implications as a powerful predictor of coronary artery disease and cerebrovascular disease [4]. Regardless, PAD is underdiagnosed with low primary care awareness [5, 6].

In clinical practice today, arterial diseases diagnosis necessitates angiography techniques [7-9]. These techniques are not ideally suited to affordable and convenient for arterial disease detection and severity assessment. The current gold standard is the digital subtraction angiography, which is an invasive technique. Other non-invasive imaging-based angiography techniques including the computed tomography angiography and magnetic resonance angiography require X-ray

radiation and expensive equipment not appropriate for affordable settings. The ankle-brachial index (ABI) is a relatively low-cost technique and is widely used for diseases screening. However, it is often criticized for its limited accuracy and robustness in diagnosing PAD [10].

Machine learning (ML) is increasingly exploited in cardiovascular disease (CVD) detection and prognosis. In particular, ML has exhibited promising efficacy in heart disease detection and prediction [11-13] as well as CVD risk and CV death prognosis [14-16]. Recent reports increasingly exploit deep learning (DL) to capitalize on its ability to automatically select characteristic features, especially in conjunction with medical imaging techniques [17-19]. In contrast to the large body of existing work on ML-based CVD detection and CV mortality prediction, relatively small number of work on ML applications to PAD is available, including detection and mortality prognosis using electronic health record as well as genomic and imaging data [20, 21].

The analysis of arterial pulse waveforms (called hereafter the pulse waveform analysis (PWA)) may play a complementary role to ML in PAD diagnosis. Indeed, PAD alters the morphology (i.e., shape) of arterial pulse wave signals (e.g., arterial blood pressure waveform (BPW) signals) by affecting the pulse wave propagation and reflection characteristics in the arteries. Hence, PWA has the potential to outperform techniques built upon discrete fiducial points (i.e., features) in the arterial pulse wave signals (e.g., ABI) by allowing the exploitation of the arterial pulse wave signals in their entirety [22-25]. However, they shows the clear limitation that BPW is not only related with a disease occurrence, so that the people who are under same disease severity level could show different ABI value, or that the people who

show the same ABI value could be under different disease severity level. Prior works show that model-based PWA has the potential to estimate CV risk predictors [26] and diagnose CVD [23] using diametric arterial pulses. Another study illustrated the theoretical feasibility of PAD diagnosis (including detection, localization, and severity assessment) using a hybrid model- and ML-based analysis of central aortic and peripheral arterial pulses [24].

A practical advantage of PWA is that it may be relevant to affordable and high-throughput PAD screening even with arterial pulse wave signals measured at the extremity locations (e.g., arm and ankle). Since these distal pulse waveforms such as distal blood pressure waveform (called hearafter distal blood pressure waveform (BPW)), are convenient to be measured using usual devices such as cuff-device, there have been lots of studies that attempt to diagnose arterial disease with distal BPW. The mainstream of existing work on PWA with distal BPW has resorted to empirical feature selection. Hence, PWA may be combined with modern deep learning (DL) to leverage its ability for automatic feature selection [25]. Despite the complementary value of DL and PWA in advancing the diagnosis of PAD (and even other CVDs), the fusion of DL and PWA for PAD diagnosis has been pursued limitedly. In fact, the state-of-the-art of DL-based PWA appears to be limited to rudimentary classification of CV health state (e.g., hypertension, atherosclerosis, and diabetes mellitus) [27]. Hence, DL-PWA fusion is a novel conceptual idea worthy of pursuit in the context of CVD diagnosis (including PAD).

Furthermore, an obvious challenge in incorporating DL into PWA is dataset limitation constraint: naïve application of DL to PWA-based PAD diagnosis requires massive longitudinal datasets associated with PAD progression in time, which

preferably also encompass diverse anatomical and physiological characteristics as well as disease severity levels. Yet in reality, only scarce (and possibly non-longitudinal) dataset from a small number of patients associated with limited anatomical and physiological characteristics, and disease severity levels may be available. First, the dataset from the patients under scarce disease severity levels deteriorates the diagnosis and severity assessment performance of deep neural network (DNN) especially for the dataset which is under the severity levels unseen to DNN during training phase. Especially on this hallow severity range, the sensitivity and specificity could drastically decrease yielding low robustness of model. Second, the limited dataset related with limited anatomical and physiological characteristics may pose formidable challenges in training a DNN for PAD diagnosis which is generalizable to a wide range of anatomical and physiological characteristics. The morphology of the arterial pulse wave signals highly depends not only on PAD but also on the anatomical and physiological characteristics of a patient. For example, mechanical properties of the arterial wall and height of the patient can alter the shape of arterial pulse wave signals by affecting the way forward and backward traveling BP waves are superposed – mechanical properties (e.g., arterial stiffness, diameter, and thickness) by altering pulse wave velocity (PWV) and height by altering the timings of superposition even for a given PWV [28]. Hence, if a DNN is trained using scarce dataset from a small number of patients (who possibly encompass only a narrow range of anatomical and physiological characteristics), the resulting PAD diagnosis algorithm may be overfitted only to the individuals in the training dataset, while its ability to generalize to other individuals (who may exhibit a large variability in anatomical and physiological characteristics beyond the training dataset) may be deteriorated.

Meanwhile, A clinical approaches more focus on PWA with arterial pulse wave signals measured at the central locations (e.g., ascending aorta which is closest artery from a heart). These central pulse waveforms such as central blood pressure waveform (called hearafter central blood pressure waveform (BPW)), are contains rich information about dynamic cardiovascular status. The left ventricle encounters the aortic systolic pressure during systole (afterload), and the diastolic aortic pressure is the determining factor in coronary perfusion. Moreover, central arteries are directly connected to major organs, including the heart, kidneys, lungs and brain. The important charactiristics of the generative changes that associated with aging and hypertension is yielded from the distending pressure of the large elastic arteries [29, 30]. Hence, the challenges of PWA with distal BPW, which are related with individual differences from anatomical and physiological characteristics and disease severity levels, is eased since it is close to the source of hemodynamic flow intrance. However, the excessive cost is required to measure the central BPW since it is commonly measured with the catheterization which is invasive measurement. The invasive method is conducted under anesthesia in a surgery operating room, it results in not only financial cost but social cost such as large time comsumption and low accessibility. Arternatively, the non-invasive method such as ultraconic device is proposed [30], but still it is quite more expensive to be measured compared to the distal BPW measurement.

Therefore, there are three great needs for PWA based arterial disease diagnosis with distal BPW using DNN. 1) How to overcome the sparsity of disease severity levels given in training phase? 2) How to compensate the sparsity of anatomical and physiological characteristics beyond the training dataset? 3) How to gather the

central BPW accurately with non-expensive way, such as measurement of distal BPW?

1.2 Research Scope and Overview

This doctoral dissertation aims at advancing three essential and co-related research areas to enable the DNN based arteria disease diagnosis with high accuracy using distal BPW: (1) Research Thrust 1 – a mutually-informed neural network for severity assessment of arterial disease to overcome the sparsity of disease severity levels given in training phase; (2) Research Thrust 2 – a continuous-property adversarial regularization for individuality independency to overcome the sparsity of anatomical and physiological characteristics beyond the training dataset; (3) a sequence-oriented neural network for inference of central BPW to gather the central BPW accurately with non-expensive way.

Research Thrust 1: A Mutualy-Informed Neural Network for Severity Assessment of Arterial Disease to Overcome The Sparsity of Disease Severity Levels Given In Training

Research Thrust 1 proposese the following two topics. One is an initial proof-of-concept of deep learning-based arterial pulse waveform analysis for affordable and convenient arterial disease screening as well as presents challenges that must be addressed for real-world clinical applications. As a preliminary study, the PAD diagnosis problem is investigated, and a deep convolutional neural network capable of detecting and assessing the severity of PAD based on the analysis of brachial and ankle arterial pulse waveforms is constructed, evaluated, and compared with the state-of-the-art ankle-brachial index (ABI) using the virtual patients. To investigate the efficacy of the DNN implementation, the visualization and latent

feature space analysis of DNN is conducted. The other is a method to training DNN-based diagnosis model with dataset under sparse PAD severity using mutualy information. The generative model is designed to compensate the sparse dataset, and the generative model and the diagnosis model are trained simultaneously and adversarily. The mutual information among latent code, which is an input of the generative model, generated data, and disease severity of known dataset is maximized to generate the data under desired disease severity level and finally maximize the performance of the diagnosis model.

Research Thrust 2: A Continuous-Property Adversarial Regularization for Individuality Independency to Overcome The Sparsity of Anatomical and Physiological Characteristics Beyond The Training Dataset

Research Thrust 2 proposes a continuous property-adversarial regularization (CPAR) approach to robust generalization of a DNN against scarce anatomical and physiological characteristics of datasets. Inspired by domain-adversarial learning [31], the conventional discrete domain-adversarial regularization to enable regularization and generalization of a DNN across multiple continuous properties by reformulating the anti-domain classification formalism used in discrete domain-adversarial regularization to a novel anti-property regression formalism applicable to multiple continuous properties. The variation of continuous anatomical and physiological characteristics is discretized and defined as dispersed different domains, and all domain-adversrial learning is conducted. In this way, the

proposed approach fosters the exploitation of latent features that can facilitate the intended task independently of confounding property-induced disturbances, by regularizing the extraction of disturbance-dependent latent features in the network's feature extraction layer.

Research Thrust 3: A Sequence-Oriented Neural Network for Inference of Central BPW to Gather The Central BPW Accurately with Non-expensive Way

Research Thrust 3 proposes a sequence-oriented neural network to robust inference of central BPW by modulating distal BPWs. Inspired by Wavenet [32], which is applied for modulation of waveform data surprisingly decrease computational cost by utilizing CNN architecture, conserving sequential characteristics. The conventional central BPW inference is conducted with hemodynamic model and its transfer function (TF), which shows low inference accuracy. The sequence-oriented neural network is composed of two sub-networks; CNN and RNN based subnet. The specialized layers in CNN based subnet, single-sided layer, masked layer, and bottle-neck layer, are proposed for sequence-oriented computation. The processed data is finally modulated in RNN based subnet. In this way the proposed approach fosters the exact central BPW inference by causal and computationally feasible way.

1.3 Dissertation Layout

This doctoral dissertation is organized as follows. Chapter 2 introduces a transmission line model for BPW data and method to induce PAD. Chapter 3 proposes a proof-of-concept and challenges of detection and severity assessment of PAD via deep learning based PWA (Research Thrust 1). Chapter 4 presents a mutualy-informed neural network for overcoming sparsity of disease severity levels by generating virtual data with desired disease level. Chapter 5 presents a strategy of continuous-property adversarial learning which overcome the continuously varying domain difference, which is, in this case, anatomical and physiological difference of individual. Chapter 6 presents a method to infer the central BPW by modulating distal BPWs via sequence-oriented neural network. Finally, Chapter 7 summarizes the doctoral dissertation with its contributions and suggests future research directions.

Chapter 2

Transmission Line Model

2.1 Transmission Line Model of Arterial Hemodynamics

A multi-branch transmission line (TL) model of arterial hemodynamics developed in a prior work [33] is used to simulate the BPW with the considerations. In brief, the human systemic arterial tree is proposed with the input impedance, and the model is composed of 55 transmission line model (Figure 2-1), each of which represents an arterial segment characterized by segment-specific viscous, elastic, and inertial properties. The arterial tree is described as a single linked list nad the input impedance ot the arterial tree is obtained by the recursive algorithm.

In each TL, the propagation of arterial blood pressure (BP) and flow (BF) waves is dictated by the propagation and reflection constants as well as the arterial length:

$$p_O = p_I\,(1+\Gamma)/\left(e^{\gamma l}+\Gamma e^{-\gamma l}\right) \tag{2.1}$$

$$q_O = q_I\,(1-\Gamma)/\left(e^{\gamma l}-\Gamma e^{-\gamma l}\right) \tag{2.2}$$

where p_I and p_O are BP waves at the inlet and outlet of the artery, q_I and q_O are BF waves at the inlet and outlet of the artery, γ is the propagation constant, Γ is the reflection constant, and l is the arterial length. BP and BF waves at the inlet

of the artery are related by the input impedance of the arterial segment:

$$p_I = q_I Z_I = q_I Z_C \left(e^{\gamma l} + \Gamma e^{-\gamma l}\right) / \left(e^{\gamma l} - \Gamma e^{-\gamma l}\right) \tag{2.3}$$

where Z_I and Z_C are the input impedance and characteristic impedance of the artery, respectively. The characteristic impedance is derived by Womersley [34] as follow;

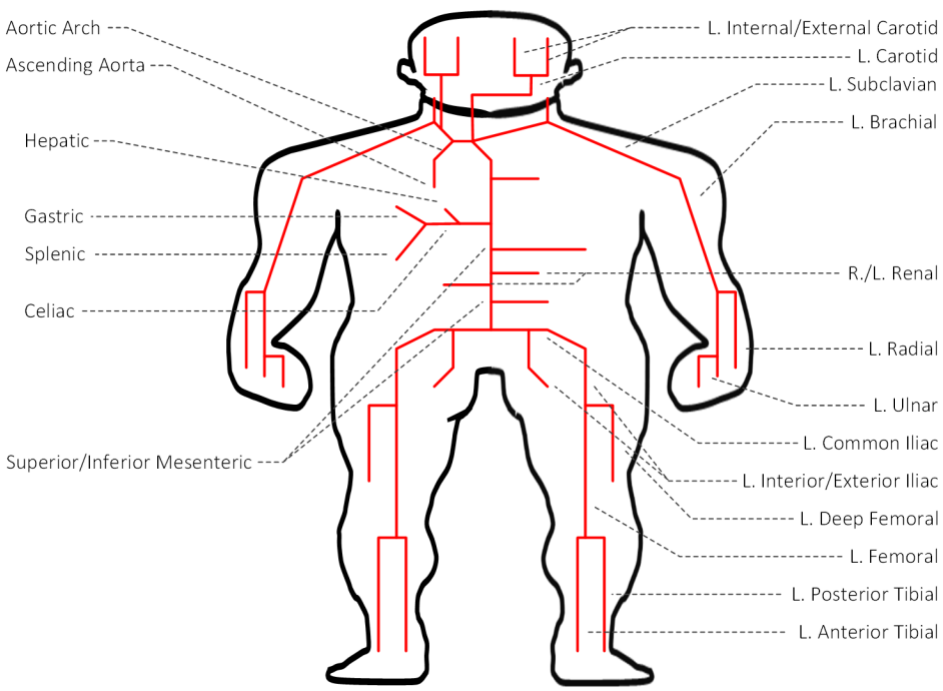

Figure 2-1 Transmission line (TL) model of arterial hemodynamics consisting of 55 TLs, each of which represents an arterial segment characterized by segment-specific viscous, elastic, and inertial properties.

$$Z_c = \frac{\rho c_0}{\pi r^2}(1-\sigma^2)^{-\frac{1}{2}}(1-F_{10})^{-\frac{1}{2}}e^{\frac{j\phi}{2}} \tag{2.4}$$

where ρ is blood density, σ is the Poisson's ratio of the artery wall, and ϕ is the phase difference. c_0 is pulse wave velocity defined by the Moens-Korteweg equation, and the propagation constant γ is described as;

$$c_0 = \sqrt{\frac{Eh}{\rho D}} \tag{2.5}$$

$$\gamma = \frac{j\omega}{c_0}(1-\sigma^2)^{\frac{1}{2}}(1-F_{10})^{-\frac{1}{2}} \tag{2.6}$$

where E is the static Young's modulus of the arterial wall, h is the arterial wall thickness, and D is the internal diameter.

If an arterial segment is terminated by a bifurcation, its load impedance is given by the parallel connection of the input impedances associated with the two descendent arteries. If an arterial segment is connected to a single descendent artery, its load impedance is given simply by the input impedance associated with the descendent artery. If an arterial segment itself is a terminal artery connected to a peripheral load, its load impedance is given by the impedance associated with the load. This model was validated with physiological data and the results of other studies, and was used in the study of arterial stenosis and arterial viscoelasticity [24, 35, 36].

2.2 Creation of Virtual PAD Patietns

A large number of virtual patients is created to investigate the potential and challenges in DL-based PWA for PAD diagnosis using the aforementioned multi-branch TL model. To create realistic virtual patients, 3 layers of variabilities are considered: inter-individual, intra-individual, and PAD severity.

First, the inter-individual variability in the arterial hemodynamics associated with the virtual patients is considered by widely varying 5 anatomical and physiological parameters in the multi-branch TL model: arterial length, diameter, and thickness, arterial elasticity, and peripheral load resistance. These parameters were varied around the nominal values reported in [33] which resulted in various virtual patients associated with the combinations of 5 distinct arterial hemodynamic properties.

Second, the PAD severity variability in each virtual patient is considered by widely varying the degree of the artery occlusion in the multi-branch TL model. In this exploratory work, the PAD occurring in the abdominal aorta is focused on, which is one of the most common PAD sites. In each of virtual patients, PAD is included by varying diameter associated with the abdominal aorta. PAD severity is considered with the range of 0% to 80% which is a range keeping the consistency with clinical report, where severity is measured as the degree of artery area occlusion (0% implies no occlusion while 100% implies complete occlusion). This resulted in various virtual patients, associated with distinct arterial hemodynamics and PAD.

Third, the intra-individual variability in the arterial hemodynamics in each virtual patient is considered to account for the uncertainty due to model imperfection

as well as random anatomical and physiological variations. It is assumed that the 5 anatomical and physiological parameters in the multi-branch TL model used to account for the inter-individual arterial hemodynamic variability have log-normal distributions around the individual-specific values as mean values with coefficient of variation of 0.01 in each virtual patient.

Then, arterial BP and BF waveforms associated with each of samples are created by inputting a representative heart blood flow waveform used in [33] (Figure 2-2) to the multi-branch TL model characterized by the sample-specific anatomical and physiological parameters (including PAD severity).

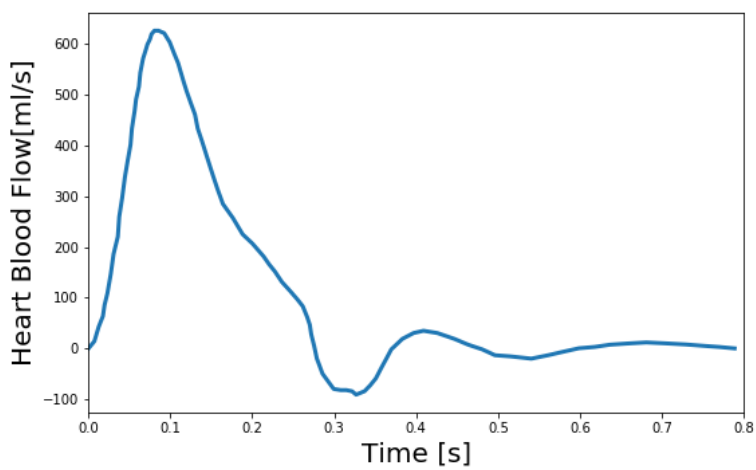

Figure 2-2 Representative heart blood flow waveform used as input to the multi-branch transmission line (TL) model of arterial hemodynamics associated with virtual patients.

2.3 Validity of Virtual Patients

The virtual patients created with the multi-branch TL model of arterial hemodynamics could reproduce the clinically observed trends in the shape of the arterial pulse waveforms in response to varying degree of PAD severity. In particular, the multi-branch TL model predicted that ankle BP pulse undergoes the following morphological changes with an increase in the PAD severity level: (i) systolic peak flattens; (ii) secondary diastolic peak disappears; (iii) pulse amplitude decreases; (iv) crest time (time interval between diastolic trough and systolic peak) increases; and (v) pulse width at half amplitude increases (Figure 2-3). It also predicted that brachial pulse amplitude increases, which contributes to a decrease in ABI with an increase in the PAD severity level. These predictions are consistent with a number of existing clinical observations [37-42] at least from qualitative standpoint. In sum, it was concluded that the virtual patients used in the proposed work can produce realistically plausible arterial pulse waveforms with respect to varying degree of PAD severity, which provided a solid basis to investigate the strengths and weaknesses of the proposed DL-based PWA approach to PAD screening and diagnosis especially in comparison with the widely used ABI technique.

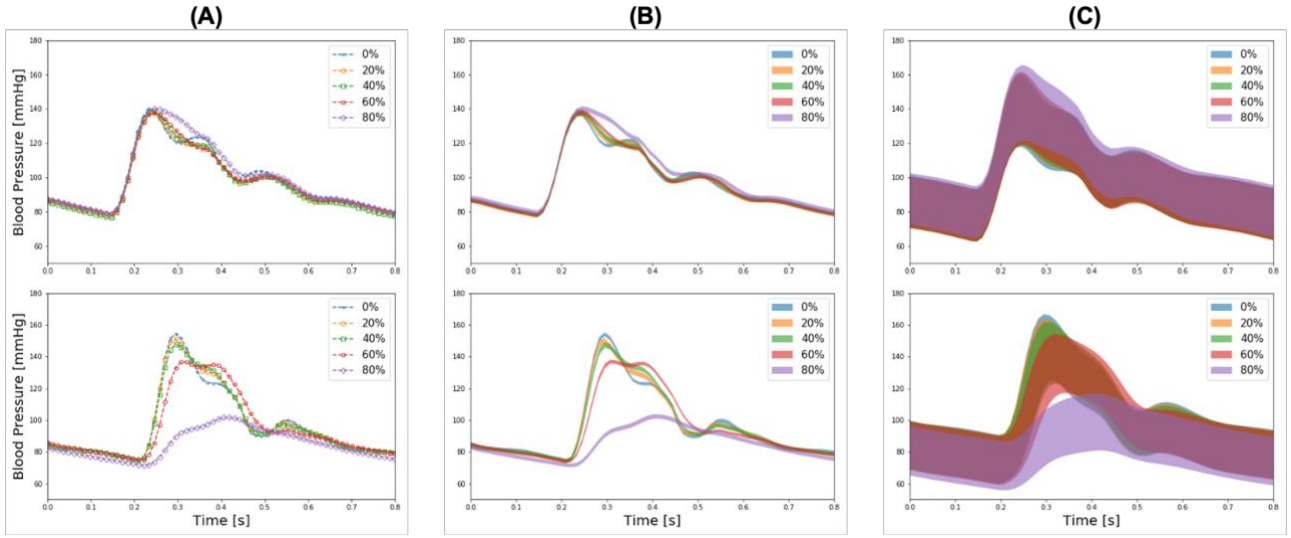

Figure 2-3 Brachial (upper panel) and ankle (lower panel) blood pressure (BP) waveforms corresponding to (A) nominal virtual patient, (B) nominal virtual patient with intra-individual variability, and (C) all the virtual patients with inter- and intra-individual variability in the test dataset, all associated with varying PAD severity. N denotes the number of arterial BP and BF waveform samples.

Chapter 3

Deep Learning based PAD Detection and Severity Assessment

DL-based PWA approach to PAD diagnosis is developed using the training and validation datasets constructed in Section 2. Specifically, a deep CNN that can predict PAD severity by the analysis of arterial pulse waveforms is constructed. In particular, brachial and ankle BP waveforms is selected as inputs to deep CNN in order to make the approach compatible to the state-of-the-art ABI technique, so that (i) the proposed approach and ABI can be directly compared and (ii) the potential for real-world application of the proposed approach is maximized.

3.1 PAD Diagnosis via Deep Learning-Based BPW Analysis

The proposed deep CNN was built upon the AlexNet [43], which was regarded as appropriate in dealing with 1-D arterial pulse waveforms associated with less complexity than 2-D images relative to other deeper CNN architectures such as ResNet [44] and DenseNet[45]. To obviate extensive tuning of hyper-parameters, the original AlexNet architecture is adopted (5 convolution layers and 3 fully connected layers), but with modest modifications (Figure 3-1).

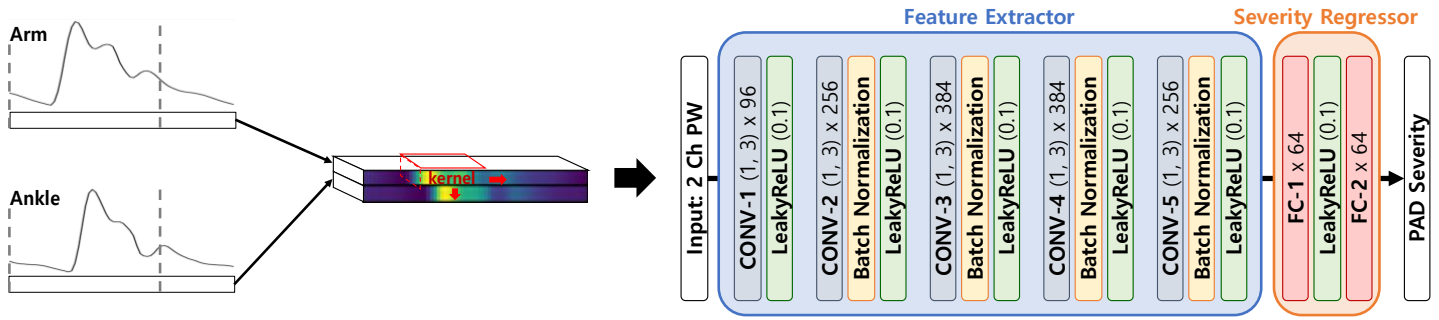

Figure 3-1 Deep convolutional neural network (CNN) architecture for PAD diagnosis via deep learning-based arterial pulse waveform analysis. *CONV-n (h, l)* × *k*: n^{th} convolution layer with height *h*, length *l* and the number of kernel *k*. LeakyReLU (a): LeakyReLU activation with slope a on negative inputs. *FC-n* × *m*: n^{th} fully-connected layer with the number of node *m*.

First, the LeakyReLU is employed as the activation function for the entire network to promote stable convergence in the training phase (Goodfellow et al., 2016). Second, batch normalization is employed in all the convolution layers to promote stable back propagation of gradient as well as regularization (Goodfellow et al., 2016). Third, the size of the fully connected layer is reduced to 64 to match it to the number of latent features outputted by the last convolution layer in the proposed CNN. Using the network architecture thus specified, the deep CNN is constructed in such a way that brachial and ankle arterial pulses are convoluted independently (Fig. 3). For this purpose, brachial and ankle arterial pulses undergo channel-wise concatenation so that these arterial pulses can be convoluted separately from each other by a shared kernel in the convolution layer. In this way, discriminative features of PAD severity embedded in the brachial and ankle arterial pulses can be extracted independently while computational efficiency can be gained with the use of shared kernels. In addition, mutual interactions between the discriminative features associated with the two arterial pulses can be exploited in the fully connected layer of the network.

3.2 Training and Evaluation Strategy

3.2.1 Configuration of Dataset

As described in Section 2, a large number of virtual patients is simulated to considering inter-/intra-individual differences and PAD severity levels. First, the inter-individual variability is considered by widely varying 5 anatomical and physiological parameters in the multi-branch TL model: arterial length, diameter, and thickness, arterial elasticity, and peripheral load resistance. These parameters were varied up to +/-20% around the nominal in an increment of 10%, which resulted in a total of 55=3125 virtual patients associated with 55 distinct arterial hemodynamic properties. Second, the PAD severity variability is considered in each virtual patent by widely varying the degree of the artery occlusion in the multi-branch TL model. In each of the 3125 virtual patients, we included PAD by varying diameter associated with the abdominal aorta. PAD severity of 0% to 80% in an increment of 10% for training and validation datasets and in an increment of 1% for test dataset is considered. This resulted in a total of 3125×9=28125 virtual patients, associated with distinct arterial hemodynamics and PAD, as the basis to construct training and validation datasets and 3125×81=253125 virtual patients, associated with distinct arterial hemodynamics and PAD, as the basis to construct test dataset. Third, the intra-individual variability is considered by assuming that the 5 anatomical and physiological parameters in the multi-branch TL model used to account for the inter-individual arterial hemodynamic variability have log-normal distributions around the individual-specific values as mean values with coefficient of variation of 0.01 in each virtual patient. Finally, the training and validation datasets are by sampling 100 and 10 times from each of the 28125 virtual patients equipped with random anatomical and physiological variations, and likewise constructed test

dataset by sampling 10 times from each of the 253125 virtual patients equipped with random anatomical and physiological variations. In this way, training and validation datasets were composed of 2812500 and 281250 arterial BP and BF waveform data samples corresponding to 28125 virtual patients, while test dataset was composed of 2531250 arterial BP and BF waveform data samples corresponding to 253125 virtual patients.

3.2.2 Training of Neural Network

To train the deep CNN, NVIDIA Titan Xp GPU and PyTorch libraries are used. The mean squared error loss between the true versus model-predicted PAD severity is used as the cost function. ADAM optimization (α=0.9, β=0.999) is used with initial learning rate of 0.0002. To assess the robustness of the deep CNN, the sensitivity of the cost function is examined with respect to the local perturbations in the hyper-parameters such as the number and the size of kernel in the convolution layer. (In detail, the sensitivity is examined by a) 1.5 and 2 times increasing the number of kernel and b) increasing the size of kernel by 1 and 2 more) Note that the deep CNN thus trained with the above regression cost can be used to both detect and assess the severity of PAD. In particular, it can be used to detect PAD simply by labeling PAD in terms of PAD severity (i.e., classifying a subject as PAD patient if the subject is associated with a pre-specified PAD severity).

3.2.3 Evaluation

The proposed DL-based PWA approach is evaluated to PAD diagnosis and

compared its efficacy with the state-of-the-art ABI technique, in terms of PAD detection and severity assessment efficacy, using the test dataset constructed in Section 3.2.2. Details follow.

First, the proposed approach is evaluated for its PAD detection performance. A range of PAD severity threshold levels is considered in labeling healthy subjects and PAD patients (10%~70%, in an increment of 10%). For each PAD labeling threshold level, 2000 virtual patients are randomly selected from test dataset (consisting of 253125 virtual patients; see Section 2.2) so that the selected patients include equal number of healthy subjects and PAD patients (i.e., 1000 healthy subjects and 1000 PAD patients; for example, in case of 40% threshold for labeling, 1000 virtual patients with <40% PAD severity were randomly chosen to form healthy subjects while 1000 virtual patients with ≥40% PAD severity were randomly chosen to form PAD patients). Then, the proposed approach and ABI technique are evaluated using the 20000 arterial BP and BF waveform data of these 2000 virtual patients (see Section 3.2.2) by (i) classifying each arterial BP and BF waveform data sample into healthy or PAD category based on the PAD severity predicted by the deep CNN when the brachial and ankle BP waveforms in the sample were inputted and the ABI value computed from the waveforms, (ii) aggregating the classification results across all the 20000 data samples associated with all the 2000 virtual patients, and (iii) computing the sensitivity and specificity as well as the accuracy of PAD detection. In the context of PAD detection, sensitivity was defined as the proportion of the 1000 PAD patient samples which were actually detected as such (with the PAD severity predicted by the deep CNN of ≥40%), while specificity was defined as the proportion of the 10000 healthy subject samples which were actually

detected as such (with the PAD severity predicted by the deep CNN of <40%). Accuracy was defined as the proportion of the 20000 test samples whose labels were classified correctly by the deep CNN.

Second, the proposed approach is for its PAD severity assessment performance. 2,000 virtual patients are randomly selected from test dataset (consisting of 253125 virtual patients; see Section 3.2.2) so that the selected patients are distributed uniformly across all the PAD severity levels (1% to 80% in an increment of 1%, which amounts to 25 virtual patients per PAD severity level). Then, the proposed approach and ABI technique are evaluated using the 20000 arterial BP and BF waveform data samples of these 2000 virtual patients (see Section 2.2), in terms of the Bland-Altman statistics between the true PAD severity versus the PAD severity predicted by the proposed deep CNN and ABI. To map ABI value to PAD severity, the ABI values is pre-calibrated to the corresponding PAD severity level based on a polynomial regression model relating ABI to PAD severity (which was obtained from the nominal virtual patient characterized by the nominal anatomical and physiological parameter values). Third, the latent feature space associated with the proposed deep CNN is analyzed using the t-distributed stochastic neighbor embedding (t-SNE) algorithm. This analysis was conducted to examine the presence of a smooth manifold relating the latent features to PAD severity. Furthermore, t-SNE is applied to visualize the input space and the space of latent features at the last convolution layer into 2-dimensional space. Then, the distributions of the input and latent features in the 2-dimensional space are investigated for a connected manifold in the direction of PAD severity. Fourth, the proposed deep CNN is analyzed using the gradient-weighted class activation

mapping (GradCAM) algorithm [46] to interpret the discriminative input features exploited by the proposed deep CNN in predicting PAD severity. GradCAM is applied to visualize the discriminative features (i.e., regions) in the brachial and ankle arterial BP waveforms which largely contributed in predicting PAD severity. Then, the physiological relevance of the input features exploited by the deep CNN in diagnosing PAD is assessed by comparing these discriminative features and the available clinical knowledge on the relationship between PAD severity and arterial pulse waveforms.

To derive a robust estimate of detection and diagnosis performance, the above evaluation is repeated 10 times and reported the average values of the sensitivity, specificity, and accuracy as well as the Bland-Altman statistics.

3.3 PAD Detection and Severity Assessment Efficacy

The proposed approach boasted robust PAD detection performance superior to the ABI technique against a wide range of PAD severity threshold levels for labeling of healthy subjects and PAD patients (Table 3-1 and Figure 3-2). Table 3-1 summarizes the PAD detection performance of the proposed approach and ABI (measured in terms of detection sensitivity, specificity, and accuracy), both corresponding to varying PAD severity threshold levels for labeling of healthy subjects and PAD patients. Figure 3-2 shows the receiver operating characteristic (ROC) curves associated with the proposed approach and ABI, both corresponding to varying PAD severity threshold levels for labeling of healthy subjects and PAD patients. The sensitivity, specificity, and accuracy values computed at the PAD classification threshold levels identical to the labeling threshold values (note that (i)

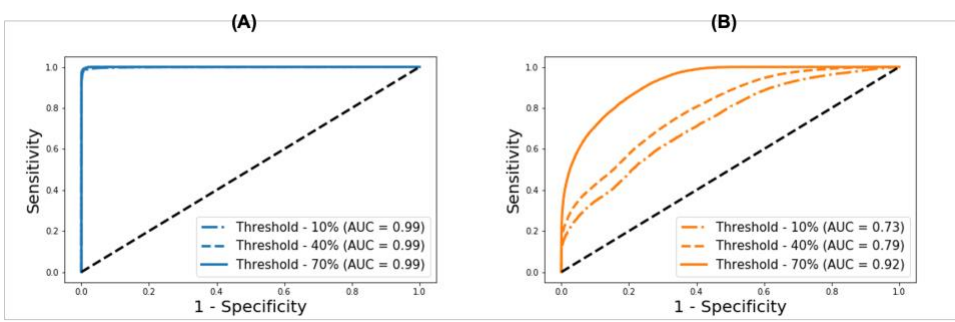

Figure 3-2 Receiver operating characteristic curves associated with the deep learning-based pulse waveform analysis approach and ankle-brachial index (ABI), both corresponding to varying PAD severity threshold levels for PAD labeling. (A) DL-based pulse waveform analysis approach. (B) Ankle-brachial index.

Table 3-1 PAD detection performance of the deep learning-based pulse waveform analysis approach and ankle-brachial index, both corresponding to varying PAD severity threshold levels for labeling of healthy subjects and PAD patients. DL: deep learning-based pulse waveform analysis approach. ABI: ankle-brachial index.

Labeling Threshold		10%	20%	30%	40%	50%	60%	70%
DL	Sensitivity	0.97	0.96	0.94	0.95	0.93	0.92	0.85
	Specificity	0.99	0.99	0.99	0.99	0.99	0.99	0.99
	Accuracy	0.99	0.98	0.97	0.97	0.96	0.95	0.91
	AUC	0.99	0.99	0.99	0.99	0.99	0.99	0.99
ABI	Sensitivity	0.96	0.94	0.73	0.64	0.60	0.58	0.59
	Specificity	0.50	0.50	0.64	0.75	0.91	0.99	0.99
	Accuracy	0.50	0.51	0.68	0.68	0.66	0.64	0.65
	AUC	0.73	0.74	0.76	0.79	0.83	0.88	0.92

the deep CNN was calibrated to the true PAD severity as part of training, and (ii) a PAD severity level can be mapped to its corresponding ABI by using the polynomial regression model relating ABI to PAD severity in Section 2.4) were consistently higher in the proposed approach than the ABI technique (Table 3-1). The proposed approach also boasted PAD severity assessment performance largely superior to the ABI technique, as indicated by its much smaller limits of agreement between the true versus predicted PAD severity levels in comparison to its ABI counterparts (Figure 3-3). Figure 3-3 shows the Bland-Altman plots between true PAD severity versus PAD severity predicted by the proposed approach and ABI. Overall, it appears that ABI is susceptible to the inter-individual variability in anatomical and physiological parameters which affect the systolic peak values associated with brachial and ankle arterial pulses, whereas the proposed approach can cope with those confounding

factors via highly sophisticated analysis of the two arterial pulse waveforms to exploit morphological characteristics beyond systolic peak values. The PAD detection and severity assessment performance remained consistent against repeated tests: the sensitivity, specificity, and accuracy values exhibited small coefficients of variation of the order of 10-3 across the 10 repeated tests outlined in Section 2.4. Lastly, the deep CNN appeared to be robust against modest perturbations in its hyper-parameters in that the alteration in the cost function with respect to the hyper-parameter perturbations considered in this work was small (<2.3%). This suggests that the AlexNet architecture used in this work was adequate, if not ideal.

The proposed approach exhibited a tendency for slight underestimation of PAD severity, especially at high PAD severity levels (Figure 3-3 (A)). This may explain its imperfect sensitivity relative to specificity at high PAD severity levels (Table 3-1), because underestimation of PAD severity in general makes the deep CNN

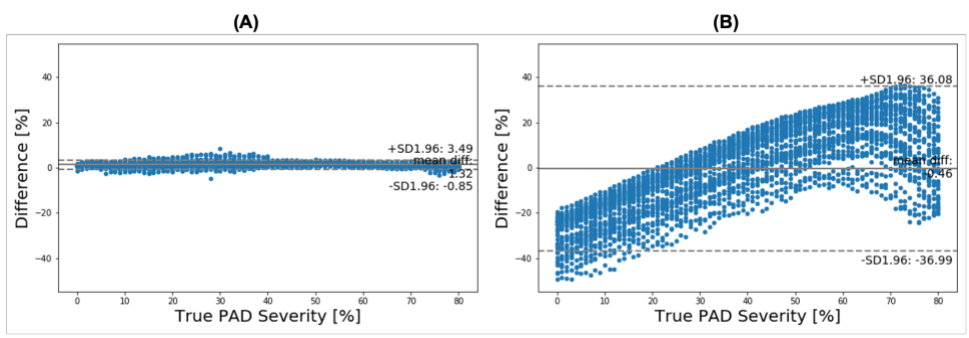

Figure 3-3 Bland-Altman plots between true PAD severity versus PAD severity predicted by (A) deep learning-based pulse waveform analysis approach and (B) ankle-brachial index (ABI).

conservative in detecting PAD. In contrast, the ABI technique suffered from a tendency for severe overestimation of PAD severity in low-severity PAD and also severe underestimation of PAD severity in high-severity PAD (Figure 3-3 (B)). This may explain its deteriorating sensitivity and improving specificity (and the suboptimal accuracy as a whole) with respect to the increase in the PAD severity level (Table 3-1). In the proposed virtual patients, ABI tended to remain at a normal constant level up to ~50% PAD severity level, beyond which it started to sharply decrease (not shown). Hence, the sensitivity of ABI is high in low-severity PAD (since it overestimates the severity in this regime) but is low in high-severity PAD (since it underestimates the severity in this regime). For the same reason, the specificity of ABI is low in low-severity PAD but is high in high-severity PAD. It is worth noting that this trend is in accordance with prior clinical observations on the low sensitivity and high specificity of ABI in detecting symptomatic PAD patients [47, 48].

3.4 Latent Feature and Interpretability Analysis

Two inherent challenges associated with DL is its susceptibility to overfitting and lack of transparency. (i) t-SNE is employed to examine if the proposed deep CNN was properly trained and (ii) GradCAM is employed to examine if the proposed deep CNN exploits appropriate input features in diagnosing PAD.

The t-SNE visualization of the input and latent feature spaces clearly illustrates that the deep CNN was properly trained to capture the relationship between the latent features extracted from the brachial and ankle pulse waveforms and PAD severity (Figure 3-4). In particular, the input feature space contains a number of small and scattered clusters associated with varying PAD severity levels (Figure 3-4 (A)), which presumably represent the inter-individual variability associated with the virtual patients. In contrast, the latent feature space clearly shows a manifold

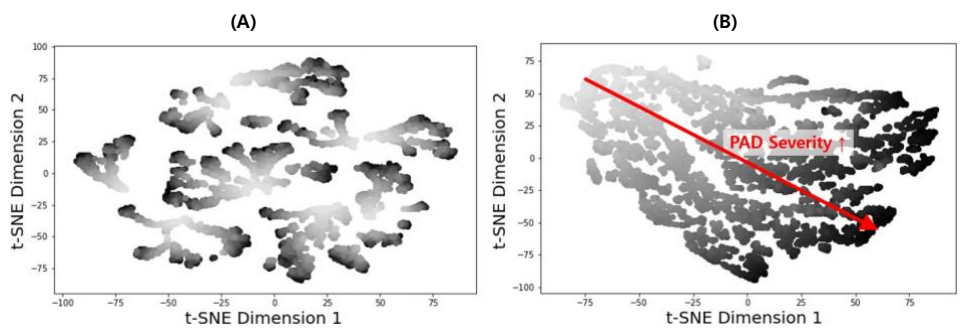

Figure 3-4 2-dimensional t-distributed stochastic neighbor embedding (t-NSE) visualization of (A) input and (B) latent feature spaces associated with the fully trained and validated deep convolutional neural network.

smoothly connecting low (upper left) to high (lower right) PAD severity levels (Figure 3-4 (B)). Hence, it may be claimed that the notable performance of the DL-based PWA approach originates from its appropriate learning of the latent features indicative of PAD severity rather than from overfitting to the data.

The discriminative input features localized by GradCAM provide support for the transparency of the deep CNN constructed in this work. Indeed, main discriminative input features included (i) the systolic up-stroke and (ii) diastolic down-stroke (including secondary peaks when exists) (Figure 3-5), which are the regions in the brachial and ankle arterial pulses in which salient morphological changes occur as PAD develops according to the existing clinical literature [37-42].

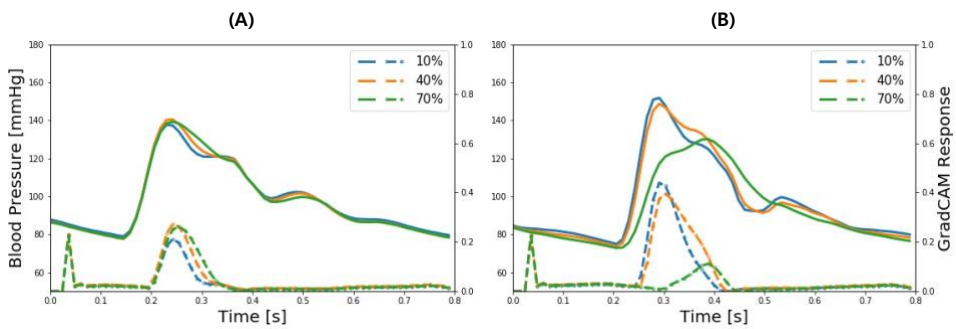

Figure 3-5 Representative brachial and ankle pulse waveforms (solid lines) and discriminative features (dotted lines) of deep convolutional neural network (CNN) localized by the gradient-weighted class activation mapping (GradCAM) associated with low (10%), medium (40%), and high (70%) PAD severity levels. (A) Brachial arterial pulse. (B) Ankle arterial pulse.

Hence, it can be claimed that the DL-based PWA approach may detect and assess the severity of PAD by analyzing brachial and ankle arterial pulse waveforms in a way similar to how experienced clinicians analyze them, although the exact mechanisms underlying how the deep CNN compiles and interprets the observed morphological changes into PAD severity are unknown.

3.5 Limitations and Opportunities

All in all, this chapter demonstrated the proof-of-concept of integrating DL and PWA for affordable and non-invasive PAD screening and diagnosis. However, this work has limitations to be addressed. In addition, this work also sheds light on outstanding opportunities toward its real clinical application.

First and foremost, this work was conducted using data collected from virtual rather than real patients. A validated multi-branch TL model was employed to create virtual patients. It is also shown that arterial pulse waveforms produced by the virtual patients exhibit the morphological characteristics observed in real PAD patients. Yet, discrepancy between virtual versus real patients may be inevitable at least to some extent, and there are a few potential sources that can obscure the initial success of this work when applied to real clinical data. In particular, the inter- and intra-individual variability considered in this work is somewhat ad-hoc. Furthermore, variability is accounted for associated only with arterial anatomical and physiological parameters but not cardiac parameters (such as stroke volume and ejection duration). In the near term, the efficacy of the proposed approach against variabilities not considered in this work may be investigated using the same virtual patients. But ultimately, future work must confirm the proof-of-concept obtained in this work using clinical data collected from real patients. Regardless of this limitation, this work may still have unique value as an exploratory study of DL-based arterial pulse waveform analysis for PAD diagnosis in a reasonably realistic yet controlled setting. Indeed, this work provides a justification for conducting a (potentially large-scale and resource-intensive) clinical data collection study for experimental investigation of DL-based PWA approaches to PAD diagnosis (and

perhaps other CVDs as well).

Second, this work was limited to the detection and severity assessment of PAD in a single arterial site. In contrast, an ideal PAD screening and diagnosis tool is required to also localize PAD. Hence, the proposed approach must be extended to a technique capable of simultaneously detecting, localizing, and assessing the severity of PAD. This requirement may present additional challenge when PAD at multiple sites with different levels of severity must be diagnosed. Future work must investigate how to extend the proposed approach to also include PAD localization capability. A possible initial strategy may be to leverage the deep CNN trained in this work in conjunction with the multi-task learning, pre-training, and continuation methods established in the DL domain so as to extend the current deep CNN to also embed the ability to localize PAD.

Third, this work assumed the availability of a large amount of data associated with a wide range of variability in anatomical and physiological characteristics as well as PAD severity levels, which may not be practically realistic. For example, the majority of PAD data may be associated with aged patients, and the proposed approach when trained with such data may not generalize well to young patients (who are associated with low PAD incidence but screening/diagnosing whom is still crucial for CV risk management). Likewise, the proposed approach when trained with data associated with one ethnic population may not generalize well to another subject to a large inter-ethnic anatomical and physiological discrepancies. Future work on coping with limited data and enormous inter-individual variability must be conducted. A possible initial strategy may be to exploit the domain adaptation and transfer techniques as well as adversarial training to guide the deep CNN work with

latent features invariant to ethnic, anatomical, and physiological characteristics.

Lastly, this work used arterial BP waveforms, which may not be easy to measure non-invasively. Practically affordable non-invasive arterial pulse waveforms (e.g., pulse volume recording waveforms [26, 38, 42] are typically measured at the skin level and thus exhibit subtle morphological differences relative to arterial BP waveforms [49]. Hence, future work must be conducted to investigate adverse effect of using non-invasive arterial pulse waveform measurements on the proposed approach as well as innovative strategies to realize the proposed approach using affordable and non-invasive arterial pulse measurements.

3.6 Conclusion

This chapter demonstrated the proof-of-concept of a novel DL-based PWA approach to PAD diagnosis. The results suggest that PAD detection and severity assessment may be feasible with data-driven analysis of arterial pulse waveforms. This work also outlined outstanding opportunities and challenges toward real-world deployment of the proposed approach, including (i) validation with data collected from real patients, (ii) PAD localization, (iii) generalizable implementation with limited data and robustness against confounding factors, and (iv) practical embodiment with affordable and non-invasive arterial pulse waveforms. Future work to explore and address these opportunities and challenges, including the development of innovative DL algorithms capable of addressing the outstanding obstacles, may serve as key cornerstones to realize affordable and convenient PAD screening and diagnosis.

Sections of this chapter have been published or submitted as the following journal articles:

1) Kim, Sooho, Jin-Oh Hahn, and Byeng Dong Youn. "Detection and Severity Assessment of Peripheral Occlusive Artery Disease via Deep Learning Analysis of Arterial Pulse Waveforms: Proof-of-Concept and Potential Challenges." *Frontiers in Bioengineering and Biotechnology* 8 (2020): 720.

Chapter 4

Mutualy-Informed Neural Network for Scarcity of Disease Severity Levels of Dataset

This chapter proposes a novel method for PAD severity assessment that uses a deep generative model to overcome a sparsity of severity levels in the training dataset. The generative model is conditioned by mutual information [50], a statistical measure of a mutual dependence, from among 1) a latent code, which is used as input, 2) the generated/real data and 3) PAD severity. Thus, the proposed approach is able to generate virtual BPW data under various/desired PAD severity scenarios, even those scenarios not found in the training phase. The severity assessment model and the generative model are trained interactively to leverage the advantages of both: the assessment model utilizes the virtual data of the generative model with its PAD severity level and the generative model is repeatedly updated using the assessment model.

4.1 Related Works: A Generative Adversarial Nets and Mutual Information

The generative model is trained to find the likelihood distribution of the dataset by disentangling the representation. Among various candidate deep-generative models, the variational auto-encoder(VAE) and generative adversarial network (GAN) model have been found to be of significant research interest [51]. The VAE model has been widely studied in various purpose, and the beginning step for generative model. But it suffers for unstable convergence compared to the GAN model. The GAN model has been widely used in various fields, from image processing (e.g., super-resolution image processing) [52], image translation [53], and image generation [54]) to speech processing (e.g., speech enhancement [55]). A GAN is composed of two competitive networks, a generator and a discriminator, that play an adversarial minmax game. The discriminator $D(x)$ tries to discriminate if the given data x is real or generated; the generator $G(z)$ tries to deceive the discriminator by generating data, as much as is realistic, from noise z. The minmax game is described as follows:

$$\begin{aligned} &\min_G \max_D V(D,G) \\ &= \min_G \max_D \left(\mathbb{E}_{x\sim P(x)} \log D(x) + \mathbb{E}_{z\sim N(0;1^2)} \log\left(1 - D\left(G(z)\right)\right)\right) \end{aligned} \tag{4.1}$$

One of the interesting research projects about GAN is InfoGAN [56], which considers mutual information between the input of the generator and the generator distribution. First, the input noise of the generator is divided into two parts, which are the random noise z and the latent code c_g. The mutual information between c_g and the generator distribution is considered in the minmax game. This

consideration of mutual information is added to the minmax game of GAN as a regularizing term as:

$$\min_G \max_D V_I(D,G) = \min_G \max_D \Big(V(D,G) - \lambda_g I\left(c_g; G\big(z, c_g\big)\right)\Big) \tag{4.2}$$

where λ_g is a hyperparameter. The mutual information $I(c_g; G\big(z, c_g\big))$ is the difference between the two entropy terms, as:

$$\begin{aligned} & I\left(c_g; G\big(z, c_g\big)\right) = H\big(c_g\big) - H\left(c_g \middle| G\big(z, c_g\big)\right) \\ & = H\left(G\big(z, c_g\big)\right) - H\big(G\big(z, c_g\big)\middle| c_g\big) \end{aligned} \tag{4.3}$$

In practice, the information-regularized minmax game varies with Variational Information Maximization (Barber) by lower bounding the mutual information by defining an auxiliary distribution $Q(c_g|x)$ as an approximation of $P\big(c_g\big|x\big)$:

$$\begin{aligned} & I\left(c_g; G\big(z, c_g\big)\right) = \mathbb{E}_x\left[\mathbb{E}_{c'_{g\sim P(c_g|x)}} \log P\big(c'_g\big|x\big)\right] + H\big(c_g\big) \\ & = \mathbb{E}_x\left[\mathcal{D}_{KL}(P \parallel Q) + \mathbb{E}_{c'_g}\big[\log Q\big(c'_g|x\big)\big]\right] + H\big(c_g\big) \\ & \geq \mathbb{E}_x \mathbb{E}_{c'_g}\big[\log Q\big(c'_g|x\big)\big] + H\big(c_g\big) = L_I(G,Q) \end{aligned} \tag{4.4}$$

Thus, the information-regularized minimax game becomes:

$$\min_{G,Q} \max_D V'_I(D,G,Q) = \min_{G,Q} \max_D \Big(V(D,G) - \lambda_g L_I(G,Q)\Big) \tag{4.5}$$

where the latent code c_g is used with the noise z as an input to the generator, and the auxiliary distribution $Q\big(c_g\big|x\big)$ estimates the original latent code c_g. An interesting observation of InfoGAN is that the latent code c_g, guided with the mutual

information, captures some specific properties of the data. For example, the continuous c_g in the MNIST cases clearly represents a rotation or width of the digit. However, it is a totally unsupervised process; thus, it is impossible not only to exploit the latent code as a desired property but even to predict which property of the data is represented by c_g.

4.2 Interactive Training of The Estimation Model. And The Generative Model Using Mutual Information

To enforce c_g to represent a desired property, which is the level of PAD severity in this case, the novel generative model was propoed with the multiple chains of mutual information: one is between data $x \sim T(x|s_x)$ and PAD severity s_x where $T(x|s_x)$ is a distribution of BPW data with given severity s_x,; another is between PAD severity s_x and the latent code c_g. Then, (5) becomes:

$$\begin{aligned} \min\max V_F = \min\max \Big(& V(D,G) - \lambda_g I\left(c_g; G\left(z, c_g\right)\right) \\ & - \lambda_s I\left(s_x; T(x|s_x)\right) - \lambda_c I\left(c_g; s_x\right) \Big) \end{aligned} \tag{4.6}$$

where λ_s and λ_c are hyperparameters. First, the lower bound of the mutual information between real BPW data x and PAD severity s_x is

$$\begin{aligned} & I\left(s_x; T(x|s_x)\right) = \mathbb{E}_x\left[\mathbb{E}_{s_x} \log P(s_x|x)\right] + H(s_x) \\ & = \mathbb{E}_x\left[\mathcal{D}_{KL}(P \parallel R) + \mathbb{E}_{s_x}[\log R(s_x|x)]\right] + H(s_x) \\ & \geq \mathbb{E}_x \mathbb{E}_{s_x}[\log R(s_x|x)] + H(s_x) = L_I(T,R) \end{aligned} \tag{4.7}$$

At this point, the auxiliary distribution $R(s_x|x)$ is considered as the PAD severity estimation model, with given BPW data x. By maximizing this mutual information, it is possible to enhance the performance of the PAD severity estimation under a given PAD severity. Meanwhile, the lower bound for mutual information between the latent code c_g and the fault severity s_x is maximized as 0 when the auxiliary distribution $R(s_x|x)$ and $Q(c_g|x)$ is identical. Thus, the final minmax game is

$$\min\max V_F = \min_{G,R}\max_{D}\left(V(D,G) - \lambda_g L_I(G,R) - \lambda_s L_I(T,R)\right) \tag{4.8}$$

This minmax game is described in Figure 4-1. In the Figure 4-1, the generator and the discriminator are identical to the case of a common GAN. Further, the auxiliary distribution R is related not only to the generator distribution G but also to the distribution of data x with mutual information from both. Thus, the proposed network is trained through two interactive tasks; one task is to generate plausible data considering the latent code c_g; the other is to estimate the PAD severity of given data x by enforcing c_g to reflect s_x.

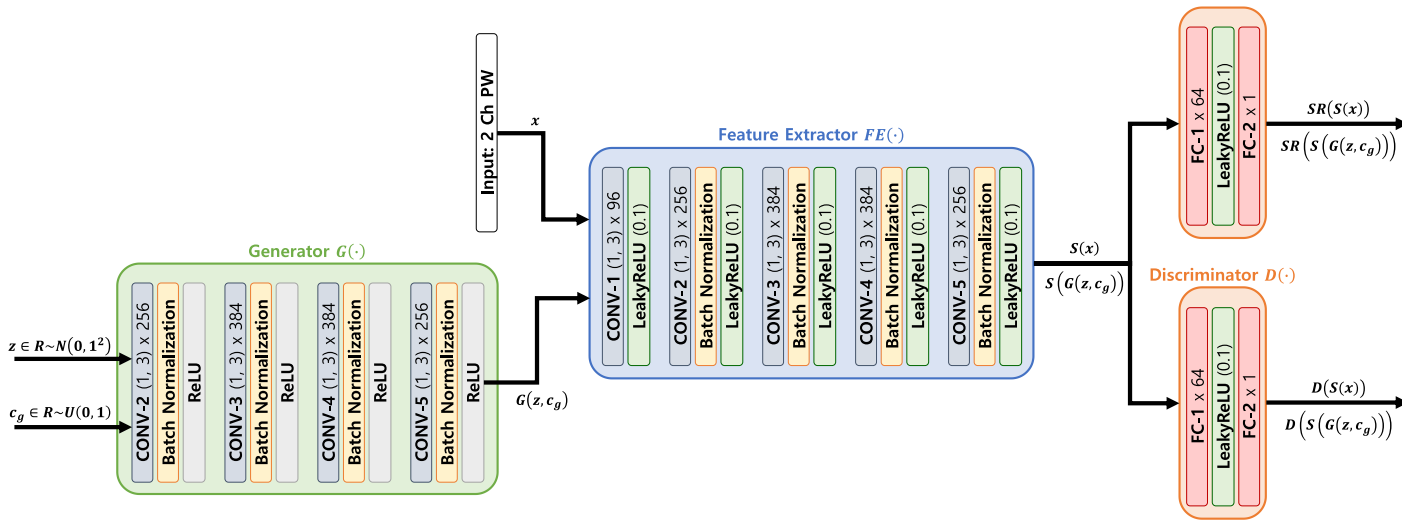

Figure 4-1 Deep convolutional neural network (CNN) architecture for PAD diagnosis via mutualy-informed deep learning-based arterial pulse waveform analysis. *CONV-n (h, l)* × *k*: n^{th} convolution layer with height *h*, length *l* and the number of kernel *k*. LeakyReLU (a): LeakyReLU activation with slope a on negative inputs. *FC-n* × *m*: n^{th} fully-connected layer with the number of node *m*.

4.3 Training and Evaluation Strategy

4.3.1 Configuration of Dataset

As described in Section 2, a large number of virtual patients is simulated to considering inter-/intra-individual differences and PAD severity levels. Similarly with Section 3.2, first, the inter-individual variability is considered by widely varying 5 anatomical and physiological parameters in the multi-branch TL model: arterial length, diameter, and thickness, arterial elasticity, and peripheral load resistance. These parameters were varied up to +/-20% around the nominal in an increment of 10%, which resulted in a total of 55=3125 virtual patients associated with 55 distinct arterial hemodynamic properties. Second, the PAD severity variability is considered in each virtual patent by widely varying the degree of the artery occlusion in the multi-branch TL model. In each of the 3125 virtual patients, we included PAD by varying diameter associated with the abdominal aorta. Unlike Section 3.2, PAD severity of 0% to 80% in an increment of *40%* for training and validation datasets and in an increment of 1% for test dataset is considered. This resulted in a total of 3125×3=9375 virtual patients, associated with distinct arterial hemodynamics and PAD, as the basis to construct training and validation datasets and 3125×81=253125 virtual patients, associated with distinct arterial hemodynamics and PAD, as the basis to construct test dataset. Since the PAD severity is quite sparse in the case of training and validation, it is challenge that although the model predict the PAD severity for training and validation dataset, it could fail for the test dataset especially for the data in hallow range of training dataset such as severity level 20% or 60%. Third, the intra-individual variability is considered by assuming that the 5 anatomical and physiological parameters in the multi-branch TL model used to account for the inter-individual arterial

hemodynamic variability have log-normal distributions around the individual-specific values as mean values with coefficient of variation of 0.01 in each virtual patient. Finally, the training and validation datasets are by sampling 200 and 10 times from each of the 9375 virtual patients equipped with random anatomical and physiological variations, and likewise constructed test dataset by sampling 10 times from each of the 253125 virtual patients equipped with random anatomical and physiological variations. In this way, training and validation datasets were composed of 1875000 and 93750 arterial BP and BF waveform data samples corresponding to 9375 virtual patients, while test dataset was composed of 2531250 arterial BP and BF waveform data samples corresponding to 253125 virtual patients.

4.3.2 Evaluation

The proposed DL-based PWA approach is evaluated to PAD diagnosis and compared its efficacy with the state-of-the-art ABI technique, in terms of PAD detection and severity assessment efficacy, using the test dataset constructed in Section 4.2.2. Details follow.

First, the proposed approach is evaluated for its PAD detection performance. A range of PAD severity threshold levels is considered in labeling healthy subjects and PAD patients (10%~70%, in an increment of 10%). For each PAD labeling threshold level, 2000 virtual patients are randomly selected from test dataset (consisting of 253125 virtual patients; see Section 2.2) so that the selected patients include equal number of healthy subjects and PAD patients (i.e., 1000 healthy subjects and 1000 PAD patients; for example, in case of 40% threshold for labeling,

1000 virtual patients with <40% PAD severity were randomly chosen to form healthy subjects while 1000 virtual patients with ≥40% PAD severity were randomly chosen to form PAD patients). Then, the proposed approach and basic DL based approach described in Section 3 are evaluated using the 20000 arterial BP and BF waveform data of these 2000 virtual patients (see Section 3.2.2) by (i) classifying each arterial BP and BF waveform data sample into healthy or PAD category based on the PAD severity, (ii) aggregating the classification results across all the 20000 data samples associated with all the 2000 virtual patients, and (iii) computing the sensitivity and specificity as well as the accuracy of PAD detection. In the context of PAD detection, sensitivity was defined as the proportion of the 1000 PAD patient samples which were actually detected as such (with the PAD severity predicted by the deep CNN of ≥40%), while specificity was defined as the proportion of the 10000 healthy subject samples which were actually detected as such (with the PAD severity predicted by the deep CNN of <40%). Accuracy was defined as the proportion of the 20000 test samples whose labels were classified correctly by the deep CNN.

Second, the proposed approach is for its PAD severity assessment performance. 2,000 virtual patients are randomly selected from test dataset (consisting of 253125 virtual patients; see Section 3.2.2) so that the selected patients are distributed uniformly across all the PAD severity levels (1% to 80% in an increment of 1%, which amounts to 25 virtual patients per PAD severity level). Then, the proposed approach and basic DL based approach described in Section 3 are evaluated using the 20000 arterial BP and BF waveform data samples of these 2000 virtual patients (see Section 2.2), in terms of the Bland-Altman statistics between the true PAD severity versus the PAD severity predicted by the proposed deep CNN and ABI.

Third, the latent feature space associated with the proposed deep CNN is analyzed using the t-distributed stochastic neighbor embedding (t-SNE) algorithm. Furthermore, t-SNE is applied to visualize the input space and the space of latent features at the last convolution layer into 2-dimensional space. Then, the distributions of the input and latent features in the 2-dimensional space are investigated for a connected manifold in the direction of PAD severity.

To derive a robust estimate of detection and diagnosis performance, the above evaluation is repeated 10 times and reported the average values of the sensitivity, specificity, and accuracy as well as the Bland-Altman statistics.

4.4 PAD Detection and Severity Assessment Efficacy

The proposed approach boasted robust PAD detection performance superior to the ABI technique against a wide range of PAD severity threshold levels for labeling of healthy subjects and PAD patients (Table 4-1 and Figure 4-2). Table 4-1 summarizes the PAD detection performance of the proposed approach and ABI (measured in terms of detection sensitivity, specificity, and accuracy), both corresponding to varying PAD severity threshold levels for labeling of healthy subjects and PAD patients. Figure 4-2 shows the receiver operating characteristic (ROC) curves associated with the proposed approach and ABI, both corresponding to varying PAD severity threshold levels for labeling of healthy subjects and PAD patients. The sensitivity, specificity, and accuracy values computed at the PAD classification threshold levels identical to the labeling threshold values (note that (i)

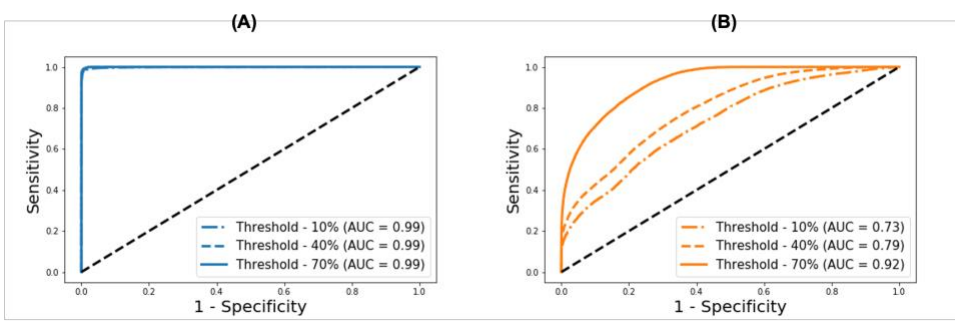

Figure 4-2 Receiver operating characteristic curves associated with the deep learning-based pulse waveform analysis approach and ankle-brachial index (ABI), both corresponding to varying PAD severity threshold levels for PAD labeling. (A) DL-based pulse waveform analysis approach. (B) Ankle-brachial index.

Table 4-1 PAD detection performance of the deep learning-based pulse waveform analysis approach and ankle-brachial index, both corresponding to varying PAD severity threshold levels for labeling of healthy subjects and PAD patients. DL: deep learning-based pulse waveform analysis approach. ABI: ankle-brachial index.

Labeling Threshold		10%	20%	30%	40%	50%	60%	70%
DL	Sensitivity	0.97	0.96	0.94	0.95	0.93	0.92	0.85
	Specificity	0.99	0.99	0.99	0.99	0.99	0.99	0.99
	Accuracy	0.99	0.98	0.97	0.97	0.96	0.95	0.91
	AUC	0.99	0.99	0.99	0.99	0.99	0.99	0.99
ABI	Sensitivity	0.96	0.94	0.73	0.64	0.60	0.58	0.59
	Specificity	0.50	0.50	0.64	0.75	0.91	0.99	0.99
	Accuracy	0.50	0.51	0.68	0.68	0.66	0.64	0.65
	AUC	0.73	0.74	0.76	0.79	0.83	0.88	0.92

the deep CNN was calibrated to the true PAD severity as part of training, and (ii) a PAD severity level can be mapped to its corresponding ABI by using the polynomial regression model relating ABI to PAD severity in Section 2.4) were consistently higher in the proposed approach than the ABI technique (Table 4-1). The proposed approach also boasted PAD severity assessment performance largely superior to the ABI technique, as indicated by its much smaller limits of agreement between the true versus predicted PAD severity levels in comparison to its ABI counterparts (Figure 4-4). Figure 4-4 shows the Bland-Altman plots between true PAD severity versus PAD severity predicted by the proposed approach and ABI. Overall, it appears that ABI is susceptible to the inter-individual variability in anatomical and physiological parameters which affect the systolic peak values associated with brachial and ankle arterial pulses, whereas the proposed approach can cope with those confounding

factors via highly sophisticated analysis of the two arterial pulse waveforms to exploit morphological characteristics beyond systolic peak values. The PAD detection and severity assessment performance remained consistent against repeated tests: the sensitivity, specificity, and accuracy values exhibited small coefficients of variation of the order of 10-3 across the 10 repeated tests outlined in Section 2.4. Lastly, the deep CNN appeared to be robust against modest perturbations in its hyper-parameters in that the alteration in the cost function with respect to the hyper-parameter perturbations considered in this work was small (<2.3%). This suggests that the AlexNet architecture used in this work was adequate, if not ideal.

The proposed approach exhibited a tendency for slight underestimation of PAD severity, especially at high PAD severity levels (Figure 4-4 (A)). This may explain its imperfect sensitivity relative to specificity at high PAD severity levels (Table 4-1), because underestimation of PAD severity in general makes the deep CNN

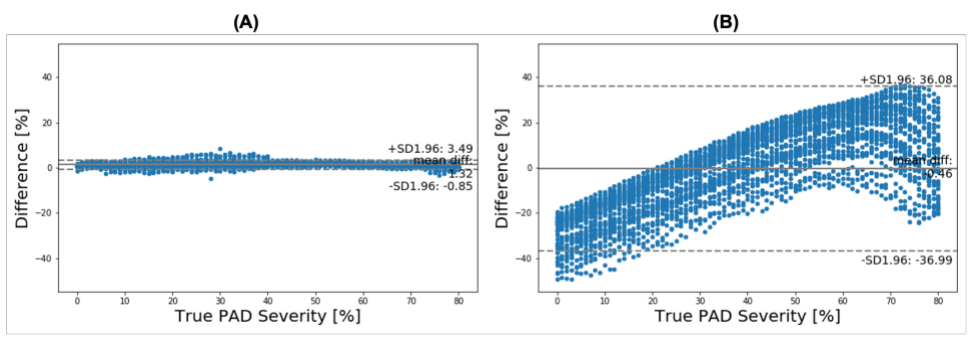

Figure 4-3 Bland-Altman plots between true PAD severity versus PAD severity predicted by (A) deep learning-based pulse waveform analysis approach and (B) ankle-brachial index (ABI).

conservative in detecting PAD. In contrast, the ABI technique suffered from a tendency for severe overestimation of PAD severity in low-severity PAD and also severe underestimation of PAD severity in high-severity PAD (Figure 4-4 (B)). This may explain its deteriorating sensitivity and improving specificity (and the suboptimal accuracy as a whole) with respect to the increase in the PAD severity level (Table 4-2). In the proposed virtual patients, ABI tended to remain at a normal constant level up to ~50% PAD severity level, beyond which it started to sharply decrease (not shown). Hence, the sensitivity of ABI is high in low-severity PAD (since it overestimates the severity in this regime) but is low in high-severity PAD (since it underestimates the severity in this regime). For the same reason, the specificity of ABI is low in low-severity PAD but is high in high-severity PAD. It is worth noting that this trend is in accordance with prior clinical observations on the low sensitivity and high specificity of ABI in detecting symptomatic PAD patients [47, 48].

4.5 Latent Feature Analysis

Two inherent challenges associated with DL is its susceptibility to overfitting and lack of transparency. (i) t-SNE is employed to examine if the proposed deep CNN was properly trained and (ii) GradCAM is employed to examine if the proposed deep CNN exploits appropriate input features in diagnosing PAD.

The t-SNE visualization of the input and latent feature spaces clearly illustrates that the deep CNN was properly trained to capture the relationship between the latent features extracted from the brachial and ankle pulse waveforms and PAD severity (Figure 4-5). In particular, the input feature space contains a number of small and scattered clusters associated with varying PAD severity levels (Figure 4-5 (A)), which presumably represent the inter-individual variability associated with the virtual patients. In contrast, the latent feature space clearly shows a manifold

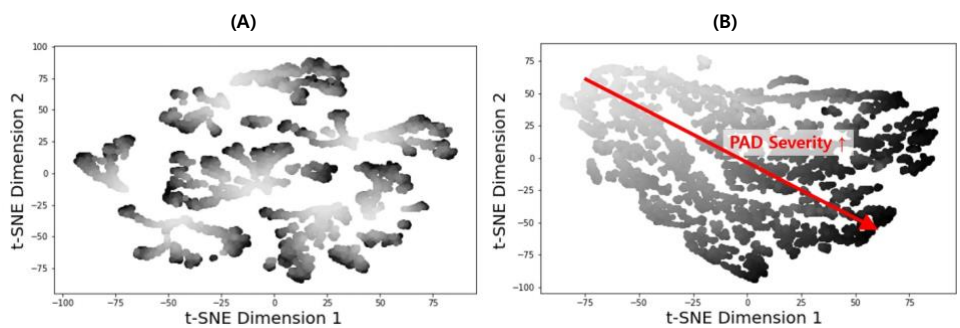

Figure 4-4 2-dimensional t-distributed stochastic neighbor embedding (t-NSE) visualization of (A) input and (B) latent feature spaces associated with the fully trained and validated deep convolutional neural network.

smoothly connecting low (upper left) to high (lower right) PAD severity levels (Figure 4-5 (B)). Hence, it may be claimed that the notable performance of the DL-based PWA approach originates from its appropriate learning of the latent features indicative of PAD severity rather than from overfitting to the data.

The discriminative input features localized by GradCAM provide support for the transparency of the deep CNN constructed in this work. Indeed, main discriminative input features included (i) the systolic up-stroke and (ii) diastolic down-stroke (including secondary peaks when exists) (Figure 4-6), which are the regions in the brachial and ankle arterial pulses in which salient morphological changes occur as PAD develops according to the existing clinical literature [37-42].

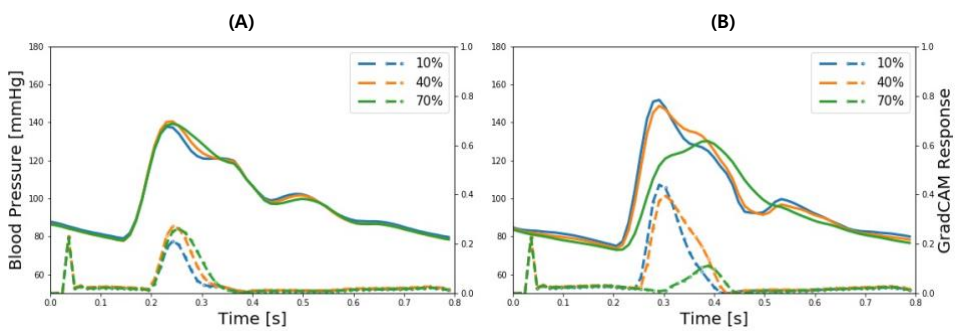

Figure 4-5 Representative brachial and ankle pulse waveforms (solid lines) and discriminative features (dotted lines) of deep convolutional neural network (CNN) localized by the gradient-weighted class activation mapping (GradCAM) associated with low (10%), medium (40%), and high (70%) PAD severity levels. (A) Brachial arterial pulse. (B) Ankle arterial pulse.

Hence, it can be claimed that the DL-based PWA approach may detect and assess the severity of PAD by analyzing brachial and ankle arterial pulse waveforms in a way similar to how experienced clinicians analyze them, although the exact mechanisms underlying how the deep CNN compiles and interprets the observed morphological changes into PAD severity are unknown.

Chapter 5

Continuous-Property Adversarial Regularization for Individuality Independency of Diagnosis Model

Current PAD diagnosis requires imaging-based methods not suited to convenient screening and surveillance purposes. In addition, the ABI technique suffers from poor diagnostic accuracy. DL-based PWA has the potential to make a leap in PAD diagnosis by virtue of its ability to automatically exploit the features indicative of PAD from readily measurable arterial pulse wave signals. Hoewever, Naïve application of deep learning to PAD diagnosis can be hampered by the fact that securing a large amount of longitudinal dataset encompassing diverse PAD severity as well as anatomical and physiological variability presents formidable challenge. The morphology of arterial pulse wave signals are influenced by anatomical and arterial mechanical characteristics as well as PAD.

Training of a deep neural network (DNN) to a small training dataset raises the risk of overfitting the PAD diagnosis algorithm only to the individuals in the training dataset while deteriorating its ability to generalize also to other individuals who may exhibit a large variability in anatomical and physiological characteristics beyond the training dataset. If combined with only scarce dataset from a small number of patients (who possibly encompass only a narrow range of anatomical and

physiological characteristics) available for training of CNN, these confounding factors can deteriorate the training of CNN by increasing the risk of the CNN overfitted only to the individuals in the training dataset while deteriorating its generalizability to unseen individuals who may exhibit more diverse anatomical and physiological characteristics beyond the training dataset. To overcome these obstacles, a continuous property-adversarial regularization (CPAR) approach is proposed in this chapter to robust generalization of a DNN against scarce datasets. The proposed approach fosters the exploitation of latent features that can facilitate the intended task independently of confounding property-induced disturbances, by regularizing the extraction of disturbance-dependent latent features in the network's feature extraction layer. By training and testing a deep convolutional neural network (CNN) for PAD diagnosis using scarce virtual datasets, it is illustrated that the CNN trained by the proposed approach was superior to a conventionally trained CNN in detecting and assessing the severity of PAD against disturbances originating from diversity in the patients' height and arterial stiffness. In addition, the advantage of the proposed approach is ascertainedin efficient training and robust generalization of DNN by contrasting it to multi-task learning which promotes the exploitation (as opposed to regularization in CPAR) of disturbance-dependent latent features in fulfilling the intended tasks.

5.1 Continuous Domain-Adversarial Regularization

In circumstances in which a DNN is trained using a scarce dataset consisting of only a small number of samples, the DNN may be overfitted to the training dataset and

thus exhibit poor performance when applied to an unseen dataset whose samples are associated with properties not covered by those in the training dataset. Two alternative approaches may be employed to mitigate such a degradation in the generalization performance of a DNN: transductive learning and regularization. In transductive learning, a DNN is pre-trained with the training dataset and subsequently refined in the target dataset [57-59]. In a prior work, a CNN was pre-trained using chest X-ray images associated with adults, and then was refined using chest X-ray images associated with pediatric population for pediatric pneumonia diagnosis [60]. In another prior work, a CNN was pre-trained using digital mammography images, and then was refined using digital tomosynthesis images for breast cancer diagnosis [61]. Hence, transductive learning requires two training phases and labeled target dataset. In regularization, a DNN is trained with a regularization penalty imposed on the loss function to bias and generalize the DNN [62]. To properly bias the DNN to maximize its generalization capability, the regularization penalty must be judiciously formulated by considering the intended task and the characteristics of the dataset. Otherwise, the DNN may still be overfitted, or it may be underfitted and generalize too broadly, ultimately leading to poor performance in both training and target datasets. Regularization-based generalization has been pursued in various applications [63, 64]. For instance, a prior work on fault diagnosis of rotating machinery regularized the discriminant structure of a DNN to extract robust latent features generalizable to unseen domains [65]. In PAD diagnosis based on PWA, the morphology of arterial pulse signals (which are presented to the DNN as inputs) are influenced by PAD as well as other confounding factors, e.g., anatomical (e.g., height of a subject) and physiological (e.g., arterial biomechanical properties of a subject) characteristics of individual

patients. A unique nature of these confounding factors is that they are continuous rather than discrete. Hence, an ideal regularization penalty for training a DNN suited to PAD diagnosis based on a scarce dataset must facilitate the generalization of the DNN across a wide range of continuous disturbances. In this work, a novel regularization approach is proposed that can address such a challenge.

The proposed regularization approach is inspired by the state-of-the-art domain-adversarial learning. In domain-adversarial learning, a DNN is trained to exploit the features relevant to the task but independent of the domain via domain-adversarial training [31, 66]. This is accomplished by defining the shift between a source domain (D_S; training dataset) and a target domain (D_T; test dataset and datasets encountered in real application of the DNN) as the $\mathcal{H}$-divergence and utilizing it in training a DNN: the $\mathcal{H}$-divergence serves as a penalty term in training the feature extraction layer, where it is minimized to set the parameters in the feature extraction layer so that the consequent features are regularized and domain-independent [67, 68]. The proposed CPAR approach extends the conventional domain-adversarial training (applicable mostly to discrete and categorical domains) to continuously connected source and target domains. Consider a domain defined by a continuous parameter P:

$$P \triangleq \left\{ p \middle| \underline{p} \leq p \leq \overline{p} \right\} \tag{5.1}$$

where the lower bound $\underline{p}$ and the upper bound $\overline{p}$ specify the range of p. For a given sample x in the domain associated with $p_x \in P$, we define the source and target domains as follows:

$$D_S(p) = \{x | d(p, p_x) \leq \varepsilon\}$$
$$D_T(p) = \{x | d(p, p_x) > \varepsilon\} \tag{5.2}$$

where $d(x, y) \triangleq \tanh|x - y|$ is a distance measure between x and y, and $\varepsilon > 0$. Let the mapping in a DNN associated with the feature extraction layer, label prediction layer, and domain regression layer as $G_f(x)$, $G_l\left(G_f(x)\right)$, and $G_\eta\left(G_f(x)\right)$, respectively (Figure 5-1). Denoting the set of latent features derived from the samples in the source and target domains pertaining to $p \in P$ as follows:

$$F_S(p) = \left\{G_f(x) \middle| x \in D_S(p)\right\}$$
$$F_T(p) = \left\{G_f(x) \middle| x \in D_T(p)\right\} \tag{5.3}$$

The effective $\mathcal{H}$-idvergence $d_{\mathcal{H}}^{eff}(P)$ between $F_S(p)$ and $F_T(p)$ across the entire (source and target) domain can be derived by integrating the $\mathcal{H}$-idvergence $d_{\mathcal{H}}\left(F_S(p), F_T(p)\right)$ associated with a specific value of p over all possible values of p in the domain. Given $n_S(p)$ the number of samples from the source domain and $n_T(p)$ the number of samples from the target domain, $d_{\mathcal{H}}\left(F_S(p), F_T(p)\right)$ can be computed empirically as follows [31]:

$$\begin{aligned} & d_{\mathcal{H}}\left(F_S(p), F_T(p)\right) \\ & \triangleq 2\left\{1 - \min_{\eta \in \mathcal{H}(p)} \left[\frac{1}{n_S(p)} \sum_{i=1}^{n_S(p)} I\left[\eta\left(G_f(x_i) = 0 \middle| p\right)\right]\right.\right. \\ & \qquad \left.\left. + \frac{1}{n_T(p)} \sum_{j=1}^{n_T(p)} I\left[\eta\left(G_f(x_j) = 1 \middle| p\right)\right]\right]\right\} \end{aligned} \tag{5.4}$$

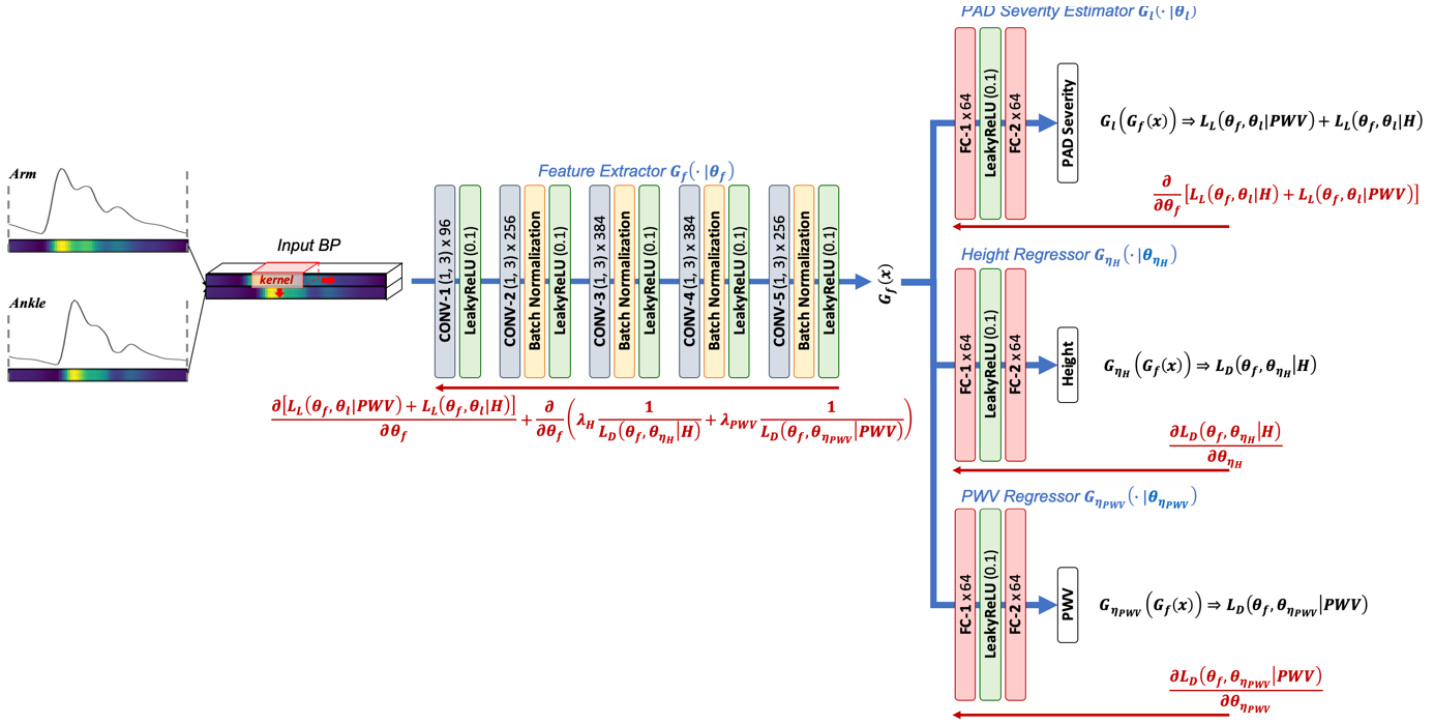

Figure 5-1 A CNN architecture for peripheral artery occlusive disease (PAD) diagnosis via CNN-based PWA.

where $\eta(\cdot\,|p)$ is a binary classifier for source vs target domains in the hypothesis class $\mathcal{H}(p)$ associated with p, while $I[\cdot]$ is an indicator (i.e., $I=1$ if the predicate is true and $I=0$ otherwise). Then, $d_{\mathcal{H}}^{eff}(P)$ is given by:

$$d_{\mathcal{H}}^{eff}(P)=\sum\nolimits_{p} d_{\mathcal{H}}\big(F_S(p),F_T(p)\big) \tag{5.5}$$

where the summation is an approximation to the integration over p. Then, it is possible to regularize the latent features against P (i.e., make them independent of P) by training a DNN so that $d_{\mathcal{H}}^{eff}(P)$ is minimized, which allows the DNN to robustly perform the intended labeling task both in the source and target domains [31]. Inspired by Eq. (5.5), we conceive the following loss function for domain regression:

$$\begin{aligned}
&L_D\big(\theta_f,\theta_\eta\big|P\big)\\
&=\sum\nolimits_{p}\left[\frac{1}{n_S(p)+n_T(p)}\sum\nolimits_{k=1}^{n_S(p)+n_T(p)} L_D\big(x_k,\theta_f,\theta_\eta\big|p\big)\right]\\
&=\sum\nolimits_{p}\left[\frac{1}{n_S(p)+n_T(p)}\sum\nolimits_{k=1}^{n_S(p)+n_T(p)}\left\{\Big(1\right.\right.\\
&\qquad\qquad -e\big(p,p_{x_k}\big)\Big)\log\frac{1}{d\left(p_{x_k},G_\eta\left(G_f(x_k)\right)\right)}\\
&\qquad\qquad \left.\left.+e\big(p,p_{x_k}\big)\log\frac{1}{1-d\left(p_{x_k},G_\eta\left(G_f(x_k)\right)\right)}\right\}\right]
\end{aligned} \tag{5.6}$$

where $e\big(p,p_{x_k}\big)\triangleq\begin{cases}1, & d\big(p,p_{x_k}\big)\le\varepsilon\\ 0, & d\big(p,p_{x_k}\big)>\varepsilon\end{cases}$, and $G_\eta\left(G_f(x_k)\right)$ is the domain regressed by the DNN when x_k is inputted. The standard 2-norm-based loss function is

employed for label prediction:

$$
\begin{aligned}
&L_L\left(\theta_f, \theta_l \middle| P\right) \\
&= \sum\nolimits_p \left[\frac{1}{n_S(p) + n_T(p)} \sum\nolimits_{k=1}^{n_S(p)+n_T(p)} L_L\left(x_k, \theta_f, \theta_l \middle| p\right) \right] \\
&\qquad = \sum\nolimits_p \left[\frac{1}{n_S(p) + n_T(p)} \sum\nolimits_{k=1}^{n_S(p)+n_T(p)} \Big(y_k \right. \\
&\qquad \left. - G_l\left(G_f(x_k)\right)\Big)^2 \right]
\end{aligned}
\tag{5.7}
$$

where y_k is the label associated with x_k. Then, training a DNN with CPAR boils down to solving the following set of optimization problems:

$$
\begin{aligned}
\theta_l^* &= \arg\min_{\theta_l} L_L\left(\theta_f, \theta_l \middle| P\right) \\
\theta_\eta^* &= \arg\min_{\theta_\eta} L_D\left(\theta_f, \theta_\eta \middle| P\right) \\
\theta_f^* &= \arg\min_{\theta_f} L_L\left(\theta_f, \theta_l \middle| P\right) + \lambda \frac{1}{L_D\left(\theta_f, \theta_\eta \middle| P\right)}
\end{aligned}
\tag{5.8}
$$

where $\lambda > 0$ is the regularization weight. It is noted that the way $L_D\left(\theta_f, \theta_\eta \middle| P\right)$ is incorporated into the training of θ_η and θ_f are distinct in Eq. (8). Indeed, given that $L_D\left(\theta_f, \theta_\eta \middle| P\right) > 0$ and its value increases as domain regression fails, θ_η can be optimized by minimizing $L_D\left(\theta_f, \theta_\eta \middle| P\right)$. In contrast, if $L_D\left(\theta_f, \theta_\eta \middle| P\right)$ is incorporated into the training of θ_f in the classical way (i.e., optimizing θ_f by minimizing $L_L\left(\theta_f, \theta_l \middle| P\right) - \lambda L_D\left(\theta_f, \theta_\eta \middle| P\right)$), then the cost function may behave poorly: (i) the loss function is no longer lower-bounded since$L_D\left(\theta_f, \theta_\eta \middle| P\right)$ can grow indefinitely, and (ii) CPAR cannot be effectively enforced when $L_D\left(\theta_f, \theta_\eta \middle| P\right) \approx 0$ because the contribution of $L_D\left(\theta_f, \theta_\eta \middle| P\right)$ to the gradient becomes negligible. Hence, the proposed loss function for training of θ_f has several advantages: (i) it is

positive and lower-bounded at zero; (ii) it is large when $L_D(\theta_f, \theta_\eta|P)$ is small, which promotes regularization by CPAR; and (iii) it gets dominated by $L_L(\theta_f, \theta_l|P)$ as $L_D(\theta_f, \theta_\eta|P)$ grows indefinitely, which promotes training of θ_η to improve the domain regression layer while minimizing the CPAR action.

It is worth mentioning that proposed CPAR approach can be readily extended to simultaneously deal with multiple domains pertaining to more than one continuous parameters $P_i \triangleq \left\{p_i \middle| \underline{p_i} \le p_i \le \overline{p_i}\right\}$, simply by connecting multiple domain regression layers to the feature extraction layer (see Figure 5-1 for a CNN with two domain regression layers). In this case, the loss functions in Eq. (5.8) are extended to the following, where N_P is the number of domain parameters:

$$\begin{aligned}
\theta_l^* &= \arg\min_{\theta_l} \sum\nolimits_{P_i} L_L(\theta_f, \theta_l|P_i) \\
\theta_{\eta_i}^* &= \arg\min_{\theta_{\eta_i}} L_D(\theta_f, \theta_{\eta_i}|P_i), \qquad i = 1, \cdots N_P \\
\theta_f^* &= \arg\min_{\theta_f} \sum\nolimits_{P_i} L_L(\theta_f, \theta_l|P_i) + \lambda_i \frac{1}{L_D(\theta_f, \theta_{\eta_i}|P_i)}
\end{aligned} \tag{5.9}$$

5.2 PAD Diagnosis Based On Continuous Property-Adversarial Regularization; Training and Evaluation Strategy

The CPAR approach in Section 5.1 is applied to the development of a CNN for PAD diagnosis under dataset limitation constraints. As shown in Figure 5-1, the CNN architecture consists of a modified AlexNet [43] structure (whose efficacy in PAD diagnosis was demonstrated in prior work [25]) combined with two domain regression layers. The CNN receives arterial pulse wave signals at an arm (brachial artery) and an ankle (tibial artery) as inputs to perform PWA and diagnose PAD. The label prediction layer predicts PAD severity. The domain regression layers are used in the training phase to maximize the extraction of features independent of two key anatomical and physiological characteristics affecting the morphology of arterial pulse wave signals and thus the efficacy of PAD diagnosis: height and arterial stiffness (using PWV as a surrogate measure).

5.2.1 Configuration of Dataset

The virtual datasets are created for training and testing of a CNN for PAD diagnosis using an established lumped-parameter mathematical model of human arterial tree based on the transmission line (TL) theory (Figure 2-1). They are created by perturbing a few anatomical and arterial mechanical parameters in the lumped-parameter mathematical model from their respective nominal values. Several parameters, such as (i) height, (ii) stiffness, diameter, and thickness of all the arteries, and (iii) resistances associated with terminal arteries, are varied. Then, the mathematical model equipped with these parameters is simulated to obtain a wide range of virtual brachial and tibial artery BP signals. Both inter-individual

variability (IIV) and intra-individual uncertainty are considered in perturbing these parameters. The IIV in height is considered in the range of 162-198cm (+/-10% perturbation with respect to nominal value). The IIV are considered in arterial diameter, thickness, and peripheral load resistance parameters of +/-20% perturbation around their respective nominal values. The IIV in arterial stiffness is considered to replicate the range of PWV observed in adults of 50-60 years in age in hypertension cohort (systolic BP>160mmHg and diastolic BP>100mmHg; PWV 4.8-15.1m/s) [31]. In combination with the IIV associated with arterial diameter, thickness, and peripheral load resistances, PWV in the range of 4.4-15.8m/s was obtained by perturbing arterial stiffness over -20%-400% of its nominal value. To create multiple arterial pulse signal samples from each virtual patient obtained with the IIVs described above, intra-individual uncertainty is considered in the form of lognormal distributions associated with the five anatomical (i.e., height) and arterial mechanical (i.e., arterial stiffness, diameter, thickness, and peripheral load resistance) parameters, with subject-specific values (nominal plus IIV) as mean and coefficient of variation of 0.01.

PAD at the abdominal aorta (which is one of the most common PAD locations) is mainly considered. To simulate PAD with increasing severity, the diameter of the abdominal aorta is decreased from its nominal value. PAD severity is defined as the degree of occlusion: 0% when normal, and 100% when fully occluded.

To create training dataset, 32 virtual patients are randomly sampled based on the IIV described above and a randomly chosen PAD severity (from within 0%-80%). From each virtual patient, 1,000 random samples are created subject to intra-individual anatomical and physiological variability by applying the intra-individual

uncertainty described above to the five anatomical and arterial mechanical parameters. Then, the mathematical model is repeatedly simulated 32,000 times by characterizing it by each of the 32,000 random parameter samples and the corresponding PAD severity levels to create brachial and tibial BP pulse signals. The resulting 32,000 arterial BP pulse signals pertaining to the 32 virtual patients along with the PAD severity, height, and PWV associated with these arterial BP pulse signals formed the training dataset.

To create test dataset, a large number of virtual patients are sampled by widely changing the IIV corresponding to the five anatomical and arterial mechanical parameters by 5% increments (5 (height: -10%, -5%, 0%, +5%, +10%) × 9 (artery diameter: -20%, -15%, … +15%, +20%) × 9 (artery thickness: -20%, -15%, … +15%, +20%) × 9 (peripheral load resistance: -20%, -15%, … +15%, +20%) × 77 (artery stiffness: -20%, -15%, … +395%, +400%) = 280,665) and PAD severity by 10% increment (from within 0%-80%). From each virtual patient at a specific PAD severity level, 10 random samples are created subject to intra-individual anatomical and physiological variability by applying the intra-individual uncertainty described above to the five anatomical and arterial mechanical parameters. Then, the mathematical model is repeatedly simulated 25,259,850 (=280,665×9 PAD severity levels) times by characterizing it by each of the 2,806,650 random parameter samples and all the PAD severity levels (0%-80%) to create brachial and tibial BP pulse signals. The resulting 25,259,850 arterial BP pulse signals pertaining to the 280,665 virtual patients along with the PAD severity associated with these arterial BP pulse signals formed the test dataset. The rationale behind creating a large-size test data was to extensively evaluate the efficacy of the proposed PAD diagnosis

approach via CNN-based PWA.

5.2.2 Training of Neural Network

The morphology of arterial pulse wave signals are influenced by confounding factors arising from anatomical and arterial mechanical characteristics as well as PAD severity. According to the Moens-Korteweg equation [28], arterial stiffness, diameter, and thickness alter the shape of arterial pulse wave signals by changing PWV (which impacts the timings with which forward and backward traveling pulse waves are superimposed [69]). In addition, height also alters the shape of arterial pulse wave signals by changing the length of pulse wave travel paths. To achieve robust PAD diagnosis accuracy irrespective of these disturbances, The CPAR approach is applied to the training of a CNN for PAD diagnosis via PWA. Prior work suggested that height and arterial stiffness exerts large influence on the morphology of arterial pulse wave signals among all the disturbances due to anatomical and arterial mechanical characteristics [25]. Hence, two domain regression layers are included in the CNN as shown in Figure 5-1, and the CPAR approach is used so that the features extracted from the brachial and tibial BP pulse signals and inputted to the label prediction layer for PAD diagnosis do not include those indicative of height and arterial stiffness.

Considering that direct non-invasive measurement of arterial stiffness is extremely challenging if not impossible, PWV is employed as a surrogate of arterial stiffness. Although PWV is dependent on arterial diameter and thickness as well as arterial stiffness [28], the observation from prior work showed that the effect of

arterial stiffness is predominant in altering the shape of arterial BP pulse signals among all the arterial mechanical properties [25], which suggests that PWV may serve as a credible surrogate of arterial stiffness.

The proposed CPAR-trained CNN-based PWA approach to PAD diagnosis for its ability to detect PAD and assess PAD severity is trained and tested using the training and test datasets outlined in Section 5.2.1. To robustly evaluate the proposed approach, The training and test datasets are repeatedly created 10 times, and the performance of the CNN is evaluated and reported the efficacy of the proposed approach in terms of the aggregated performance of the CNN obtained from the 10 tests. In training the CNN, the ADAM optimizer is used with $\alpha = 0.5$, $\beta = 0.999$. The learning rate and regularization weight (λ) are set as 0.0001 and 0.002, respectively.

5.2.3 Evaluation

The performance metrics included (i) sensitivity, specificity, accuracy, and area under the ROC curve (AUC) as the measures of PAD detection and (ii) r^2 value and root-mean-squared error (RMSE) between actual vs CNN-predicted PAD severity as the measures of PAD severity assessment, all derived using the test dataset. The detection accuracy of the proposed CPAR-trained CNN-based PWA approach is evaluated to PAD diagnosis against a number of PAD severity values as the PAD labeling threshold. To examine the advantage of PWA over conventional ABI technique, the performance metrics are compared associated with PWA and ABI. To enable objective comparison, ABI value is mapped to PAD severity via a pre-

calibrated polynomial regression model relating ABI to PAD severity (which was derived based on the virtual patient characterized by the nominal anatomical and physiological parameter values).

To scrutinize the role of CPAR in promoting the use of features independent of domain disturbances, the PAD diagnosis efficacy of the CNN trained with (i) CPAR, (ii) conventional learning without CPAR (in which no domain-adversarial regularization is enforced), and (iii) multi-task learning (which, as opposed to CPAR, fosters the exploitation of the features commonly useful for PAD diagnosis and domain regression) are compared using the test dataset. In addition, the performance of the proposed CNN-based PWA approach to PAD diagnosis is investigated with respect to the extent to which CPAR is applied, by comparing the CNN trained with CPAR applied to height only, PWV only, and both height and PWV using the test dataset. Finally, to assess the validity of PWV as a credible surrogate of arterial stiffness, the CNN with arterial stiffness used for domain regularization is also trained, and its performance is compared with the CNN with PWV used for domain regularization using the test dataset.

5.3 Efficacy of CPAR

The CNN trained with CPAR exhibited adequate PAD detection and assessment accuracy (Figure 5-2). Figure 5-2 shows (A) the receiver operating characteristic (ROC) curve and (B) the Bland-Altman plot between actual vs predicted PAD severity associated with the proposed CNN-based PWA approach to PAD diagnosis. It showed AUC consistently higher than 0.9 across all the detection thresholds considered in this work, and achieved nearly unbiased severity assessment (bias <0.1%).

Comparing the CNN trained with CPAR against the CNN trained without CPAR and another CNN trained with multi-task learning ascertained the role of CPAR in robustifying the CNN against anatomical and arterial mechanical

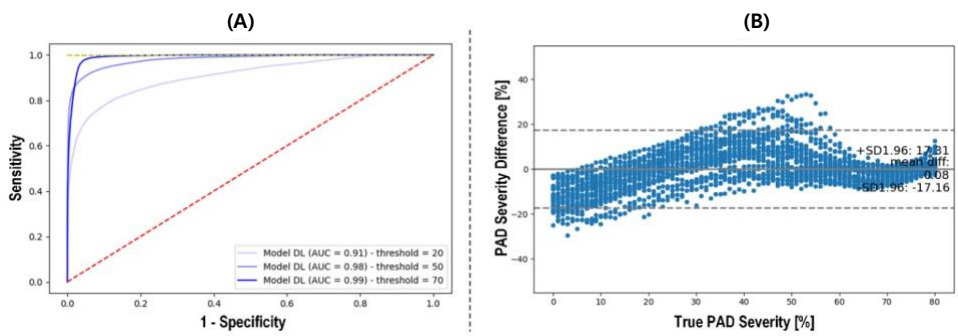

Figure 5-2 Efficacy of CNN-based PWA approach to PAD diagnosis. (A) Receiver operating characteristic (ROC) curve. (B) Bland-Altman plot between actual vs predicted PAD severity.

Table 5-1 PAD severity assessment accuracy associated with the ABI technique as well as CNN trained with (i) CPAR, (ii) conventional learning without CPAR, and (iii) multi-task learning.

	ABI	DL (NO CPAR)	DL (CPAR)	MULTI-TASK LEARNING
RMSE [%]	23.0	15.0	9.5	16.9
r^2 Value	0.034	0.588	0.834	0.478

disturbances (Figure 5-3 and Table 5-1). The CNN trained with CPAR was superior to the CNN trained without CPAR and the CNN trained with multi-task learning in both detection and severity assessment aspects. Specifically, the CPAR-trained CNN exhibited superior sensitivity while maintaining specificity comparable to its competitors (by virtue of its unbiased estimation of PAD severity, in contrast to its competitors in which PAD severity was underestimated on the average), thereby achieving superior accuracy and AUC characteristics. It is noted that the CNN trained without CPAR was superior to the CNN trained with multi-task learning. Noting that (i) the CNN trained without CPAR does not enforce any action against domain disturbances, and that (ii) multi-task learning fosters the extraction of latent features indicative of domain disturbances in performing PAD diagnosis, the results suggest that regularizing the latent features with CPAR can improve the performance of the intended task susceptible to domain-induced disturbances by making them independent of (or at least less dependent on) domain disturbances.

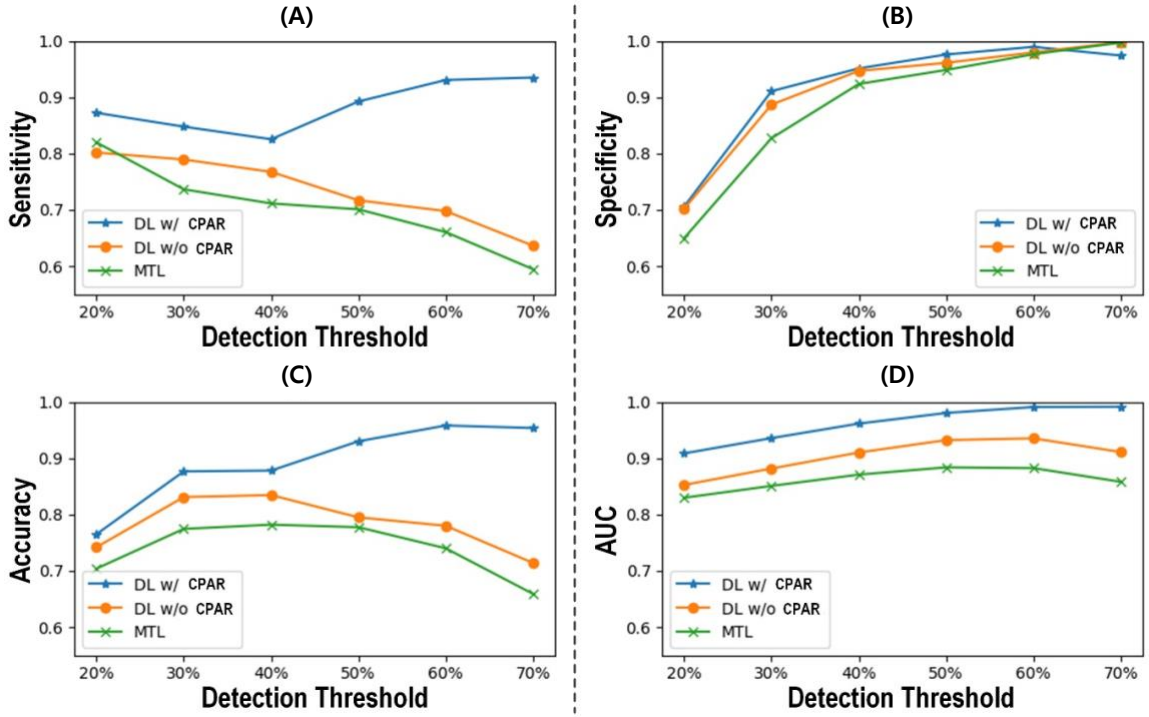

Figure 5-3 PAD detection accuracy associated with the CNN trained with CPAR, conventional learning without CPAR, and multi-task learning. (A) Sensitivity. (B) Specificity. (C) Accuracy. (D) AUC.

The advantage of CPAR may also be ascertained from the fact that the efficacy of CNN-based PWA approach to PAD diagnosis was improved as CPAR was applied simultaneously to multiple domain-induced disturbances than to one domain disturbance at a time (Figure 5-4). Figure 5-4 compares the PAD detection accuracy of the CNN trained with CPAR applied to (i) height only, (ii) PWV only, and (iii) both height and PWV. The CNN trained with CPAR to regularize against height and PWV exhibited consistently higher sensitivity than those trained to regularize only against height or PWV, despite slightly lower specificity than the height-regularized CNN (which, again, appears to be due to its unbiased estimation of PAD severity, in contrast to its competitors in which PAD severity was underestimated on the average). The CNN regularized against both height and PWV was persistently superior to the one regularized only against PWV in terms of accuracy and AUC. In terms of accuracy and AUC characteristics, the CNN regularized against both height and PWV was not consistently superior to its competitor regularized only against height. However, considering all the performance aspects (sensitivity in particular), we contend that the CNN regularized against both height and PWV may still be superior to the ones regularized only against height or PWV.

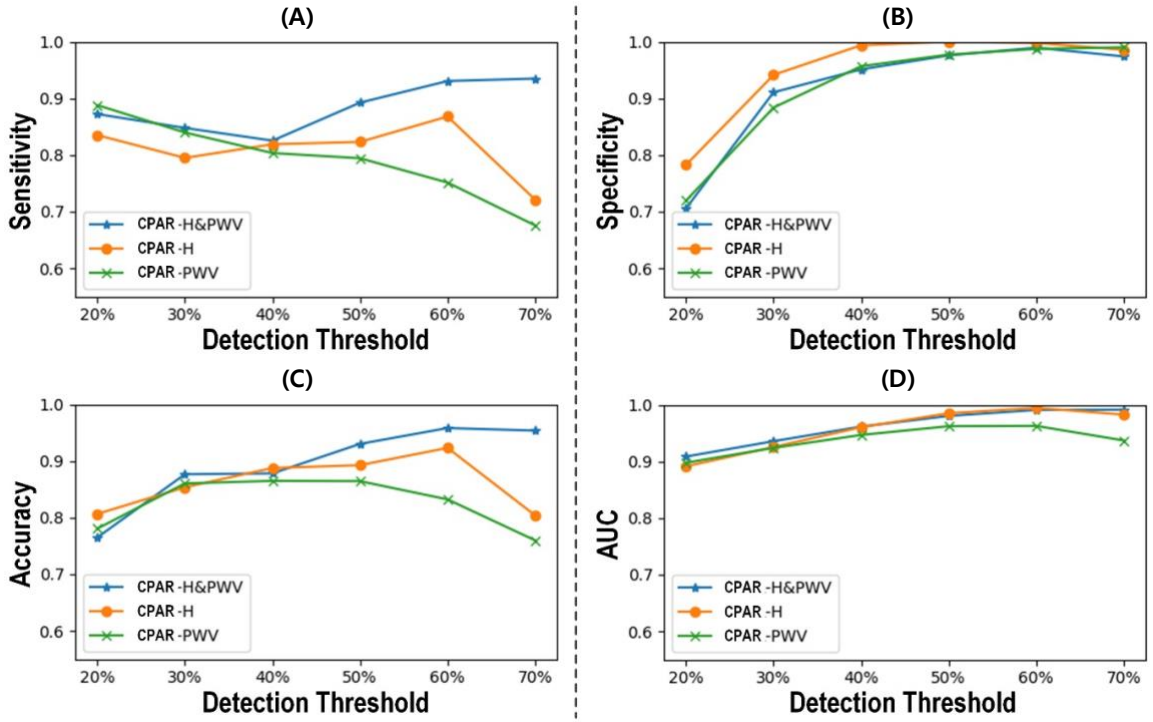

Figure 5-4 PAD detection accuracy of the CNN trained with CPAR applied to height only (H), PWV only (PWV), and both height and PWV (H&PWV). (A) Sensitivity. (B) Specificity. (C) Accuracy. (D) AUC.

All in all, the results strongly demonstrate the potential of CPAR in realizing CNN-based PWA approach to PAD diagnosis. CPAR can derive a CNN robust against anatomical and arterial mechanical properties altering the morphology of arterial BP pulse signals, by virtue of its ability to foster the exploitation of latent features independent of the domain-induced disturbances in performing PAD diagnosis task even when the dataset available for training is scarce and non-longitudinal.

5.4 Potential for Clinical Applicability

A few critical questions arise regarding the potential of the CNN-based PWA approach to PAD diagnosis for real-world clinical application: (i) is it superior to the current state-of-the-art; and (ii) does the use of PWV as a surrogate of arterial stiffness drastically impact the PAD diagnosis efficacy?

The CNN-based PWA approach to PAD diagnosis was much superior to the ABI technique in terms of both detection and severity assessment (Table 5-1). One implication is that the exploitation of the entire arterial pulse signals is more efficacious than the use of isolated fiducial points therein in diagnosing PAD. This implication justifies the complexity in the measurement and analytics required for PWA. Another implication is that the CNN-based PWA approach can leverage CPAR to improve its robustness against domain-induced disturbances due to the anatomical and arterial mechanical characteristics, whereas the ABI technique is inevitably prone to those disturbances.

The use of PWV instead of (practically unmeasurable) arterial stiffness did not largely compromise the efficacy of CNN-based PAD diagnosis (Figure 5-5). Figure 5-5 compares the PAD detection accuracy of the CNN trained with (i) PWV and (ii) arterial stiffness used for domain regularization, respectively. TABLE I summarizes the PAD severity assessment accuracy associated with the ABI technique as well as CNN trained with (i) CPAR, (ii) conventional learning without CPAR, and (iii) multi-task learning. Indeed, the former exhibited only a marginal drop in the sensitivity, accuracy, and AUC characteristics relative to the latter, while the specificity was more or less maintained. This implies that, although PWV is

not a perfect surrogate of arterial stiffness due to its reliance on other arterial mechanical properties, it may still be a viable choice to enable real-world implementation of the CNN-based PWA approach to PAD diagnosis in conjunction with CPAR-augmented learning with regularization.

All in all, the results suggest that CPAR-trained CNN-based PWA approach to PAD diagnosis may open up unprecedented opportunities for improving the convenience and accuracy of PAD screening and surveillance.

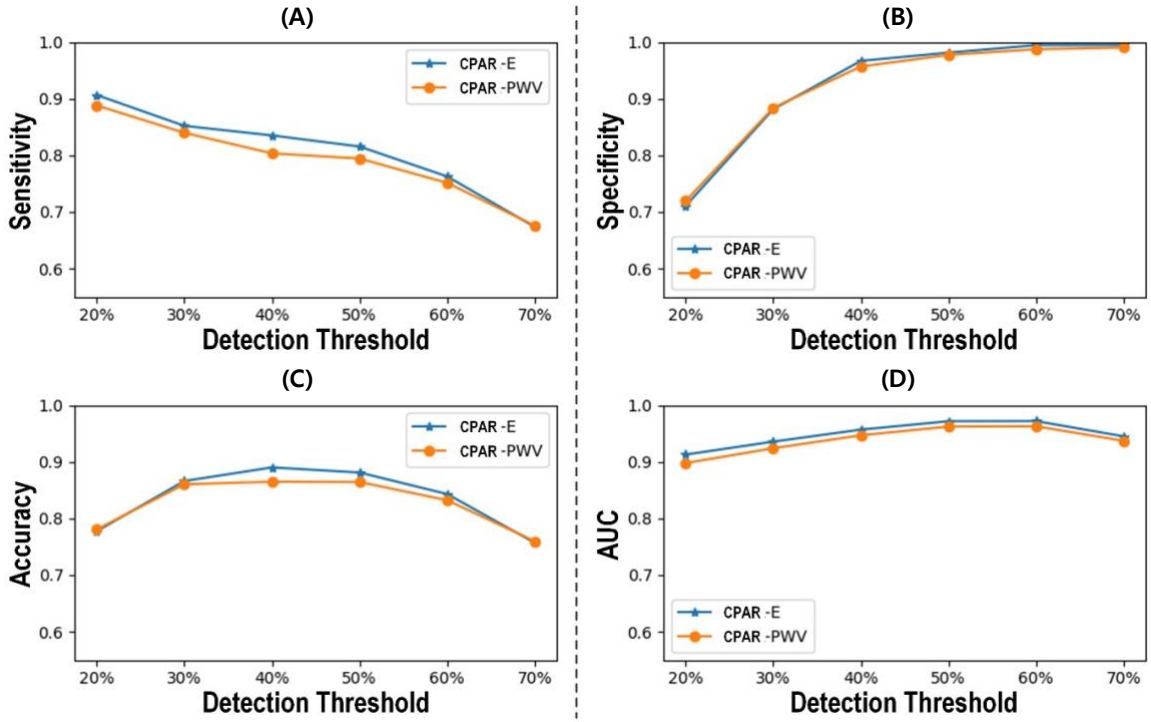

Figure 5-5 PAD detection accuracy of the CNN trained with PWV (PWV) and arterial stiffness (E) used for domain regularization.

5.5 Conclusion

In this chapter, CPAR, an enabling methodology for robust training and generalization of a DNN to detect and assess the severity of PAD against continuous property-induced disturbances arising from anatomical and arterial mechanical characteristics, is proposed. The results demonstrated the ability of the CPAR to promote the extraction of latent features independent of domain disturbances, thereby robustifying the performance of PAD diagnosis against a wide range of IIV in height and arterial stiffness. Given the proof-of-concept nature of this work based on virtual in silico dataset, future work must investigate the in vivo efficacy of the proposed PAD diagnosis approach based on CPAR-trained CNN. In addition, it may be worth investigating the potential of CPAR-trained deep learning in the diagnosis of diseases other than PAD.

Sections of this chapter have been published or submitted as the following journal articles:

1) Kim, Sooho, Jin-Oh Hahn, and Byeng Dong Youn. "Deep Learning-Based Diagnosis of Peripheral Artery Disease via Continuous Property-Adversarial Regularization: Preliminary in Silico Study." IEEE Access 9 (2021): 127433-127443.

Chapter 6

Sequence-Oriented Neural Network for Inference of Central Blood Pressure Waveform

Sequence-oriented neural network that modulate given waveform data is proposed to infer the central BPW using distal BPWs, measure at extremecity (arm and ankle). Specifically, a deep CNN modified to be optimized for sequential data processing and a deep RNN are integrated in the purpose of (i) computational feasibility and (ii) conservation of sequential characteristics. The approach is constructed upon the training and validation datasets in Section 2. The result demonstrats the ability of the inference ability of the sequence-oriented neural network preserving clinically important morphologies.

Since direct measurements are invasive and require excessive cost, the inference of central BPW using distal BPW, which can be measured non-invasively, becomes highlighted. It is conducted mathematical transformation, and the transfer function (TF) from single origin is designed and optimized based on ARX model [70]. Developing the idea, invasive central aortic pressure by micrometers and radial pressure by automatic intraocular pressure were measured and hemodynamic transitions is built [71]. The transfer function between central BPW and distal BPW could be calculated as a parametric model for each patient. Since TF varied

from patient to patient with fluctuation coefficients, the transfer functions of individuals are averaged as generalized tranfer function (GTF). However, this generalization has an inherit limitation since the identical transfer function is applied to various individuals who has different anatomical and physiological characteristics. GTF is individualized to an individualzed transfer function (ITF) from double origins, such as brachial and ankle BPW, is designed for individually optimized transfer function with higher precision [72]. In ITF, the central BPW is estimated in two steps; (i) it determins the cardiovascular circulatory dynamics, and (ii) central BPW is estimated by de-convolving peripheral circulatory waveforms. However, the model is still criticized by its robustness and inference accuracy.

6.1 Central BPW Inference via Sequence-Oriented Neural Network

The proposed sequence-oriented neural network is composed of two sub-networks considering the computation metrics; RNN and CNN based subnets. The CNN based subnet is inspired from Wavenet proposed in [32], which is designed as waveform generative model. In common, the regressive models, such as RNN, are used to process waveform data, with its sequential characteristics, and the CNN is adopted for images processing with its strength on local information extraction. However, when the depth of the neural network become deeper, the regressive models require excessive computational cost. In this background, the Wavenet is proposed th overcome the computational cost of the regressive models, still conserving the sequence-oriented regressive characteristics even with local

relational information of data.

In overall, the sequence-oriented neural network uses brachial band ankle BPWs, which are non-invasively measurable by cuff-device) as 2 channelled input, and returns single channel central BPW as output. Also, considering the characteristics of sequcntial data, the model is designed to be independent from data length (as like general sequential model based on regressive model) (Figure 6-1).

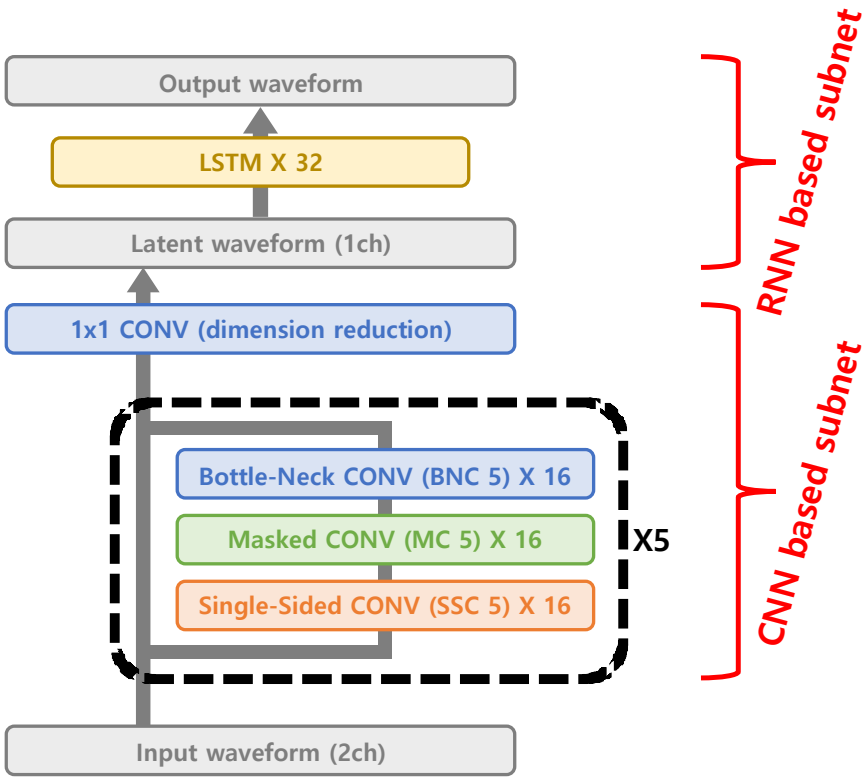

Figure 6-1 The scheme of proposed sequence-oriented neural network with two sub-networks; CNN based and RNN based subnet

The CNN based subnet of the proposed sequence-oriented neural network is composed of 4 different layer types. First, the single-sided convolution layer is proposed to preserve the causality of sequential data. Since the layer based on convolutional computation take futuristic information simultaneously because of kernel shape, the basic convolution layer is uncausal. Thus, in the single-sided convolutiona layer, the un-causal area of kernel is masked as grey zone which is not used in convolutional process, so that the yielded output conserves the causality (Figure 6-2 (A)). Second, the masked convolution layer is proposed as a skip-

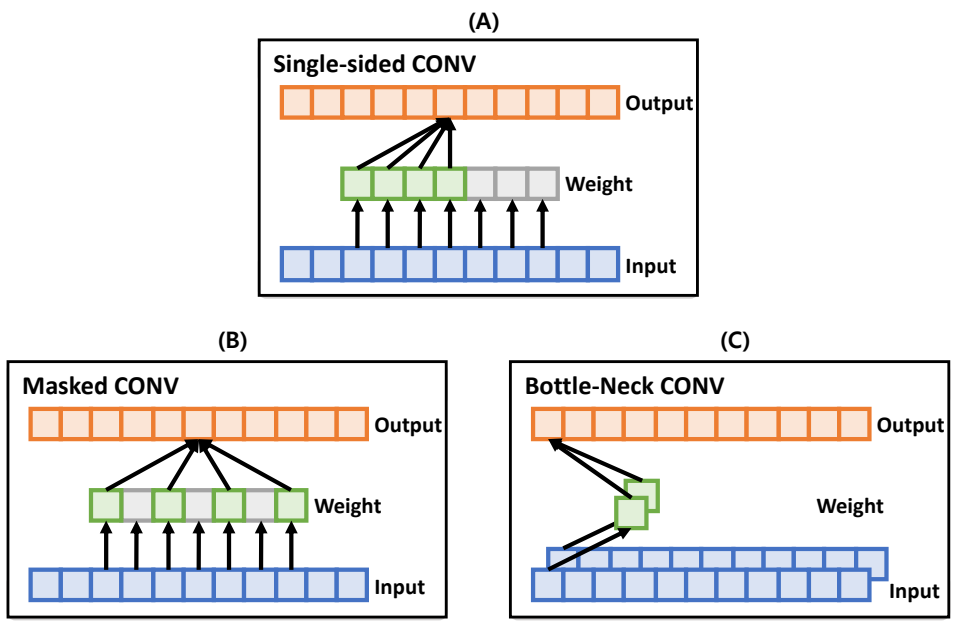

Figure 6-2 The scheme of layers of the proposed CNN based subnet; (A) single-sided convolution layer. (B) masked convolutiona layer. (C) bottle-neck convolution layer.

connection. The kernel is masked in turns, so that the kernel could reach to farther sequence data with same effective length of kernel (Figure 6-2 (B)). Third, the bottle-neck convolutional layer is imposed for dimensionality reduction in kernel-wise and preserve dimension consistency with input waveform by 1 by 1 convolution (Figure 6-3(C)). As a last, the proposed convolution layers are blocked and connected as a residual block for deep and trainable architecture [73]. The RNN base subnet of the proposed sequence-oriented network is composed with LSTM layers [74] for finalizing the sequential modulation.

6.2 Inference of Central BPW; Training and Evaluation Strategy

The sequence-oriented neural network in Section 6.1 is applied to the inference of central BPW using distal BPW measure at brachial and ankle by cuff-devices. As shown in Figure 6-1, the sequence-oriented neural network receives arterial pulse wave signals at an arm (brachial artery) and an ankle (tibial artery) as inputs to infer the cental pulse wave signal (ascending aorta). The both CNN and RNN based subnet conduct waveform modulation on causal sequence.

6.2.1 Configuration of Dataset

The virtual datasets are created for training and testing of a CNN for PAD diagnosis using an established lumped-parameter mathematical model of human arterial tree based on the transmission line (TL) theory (Figure 2-1). They are created by perturbing a few anatomical and arterial mechanical parameters in the lumped-parameter mathematical model from their respective nominal values. Several parameters, such as (i) height, (ii) stiffness, diameter, and thickness of all the arteries, and (iii) resistances associated with terminal arteries, are varied. Then, the mathematical model equipped with these parameters is simulated to obtain a wide range of virtual brachial and tibial artery BP signals. Both inter-individual variability (IIV) and intra-individual uncertainty are considered in perturbing these parameters. The IIV in height is considered in the range of 162-198cm (+/-10% perturbation with respect to nominal value with increnet 10%). The IIV are considered in arterial diameter, thickness, and peripheral load resistance parameters of +/-20% perturbation around their respective nominal values with increment 20%. The IIV in arterial stiffness is considered to replicate the range of PWV observed in

adults of 50-60 years in age in hypertension cohort (systolic BP>160mmHg and diastolic BP>100mmHg; PWV 4.8-15.1m/s) [31]. In combination with the IIV associated with arterial diameter, thickness, and peripheral load resistances, PWV in the range of 4.4-15.8m/s was obtained by perturbing arterial stiffness over -20%-400% of its nominal value with increment 20%. To create multiple arterial pulse signal samples from each virtual patient obtained with the IIVs described above, intra-individual uncertainty is considered in the form of lognormal distributions associated with the five anatomical (i.e., height) and arterial mechanical (i.e., arterial stiffness, diameter, thickness, and peripheral load resistance) parameters, with subject-specific values (nominal plus IIV) as mean and coefficient of variation of 0.01.

In addition, the inference when patients under PAD are considered together is studied for comparative study, and PAD at the abdominal aorta (which is one of the most common PAD locations) is mainly considered. To simulate PAD with increasing severity, the diameter of the abdominal aorta is decreased from its nominal value. PAD severity is defined as the degree of occlusion: 0% when normal, and 100% when fully occluded with range of 0% to 80% with increment 10%.

To create training dataset, 128 virtual patients are randomly sampled based on the IIV described above and a randomly chosen PAD severity (from within 0%-80%). From each virtual patient, 1,000 random samples are created subject to intra-individual anatomical and physiological variability by applying the intra-individual uncertainty described above to the five anatomical and arterial mechanical parameters. Then, the mathematical model is repeatedly simulated 128,000 times

by characterizing it by each of the 128,000 random parameter samples and the corresponding PAD severity levels to create central, brachial, and tibial BP pulse signals. The resulting 128,000 arterial BP pulse signals pertaining to the 128 virtual patients along with the PAD severity, height, and PWV associated with these arterial BP pulse signals formed the training dataset.

To create test dataset, a large number of virtual patients are sampled by widely changing the IIV corresponding to the five anatomical and arterial mechanical parameters (3 (height: -10%, 0%, +10%) × 3 (artery diameter: -20%, 0%, +20%)) × 3 (artery thickness: -20%, 0%, +20%) × 3 (peripheral load resistance: -20%, 0%, +20%) × 22 (artery stiffness: -20%, 0%, … +380%, +400%) = 1782) and PAD severity by 10% increment (from within 0%-80%). From each virtual patient at a specific PAD severity level, 100 random samples are created subject to intra-individual anatomical and physiological variability by applying the intra-individual uncertainty described above to the five anatomical and arterial mechanical parameters. Then, the mathematical model is repeatedly simulated 1,603,800 (=178,200×9 PAD severity levels) times by characterizing it by each of the 178200 random parameter samples and all the PAD severity levels (0%-80%) to create brachial and tibial BP pulse signals. The resulting 1,603,800 arterial BP pulse signals pertaining to the 178,2 virtual patients along with the PAD severity associated with these arterial BP pulse signals formed the test dataset. The rationale behind creating a large-size test data was to extensively evaluate the efficacy of the proposed PAD diagnosis approach via CNN-based PWA.

6.2.2 Training of Neural Network

To train the deep sequence-oriented neural network, NVIDIA Titan Xp GPU and PyTorch libraries are used. The point-wise mean squared error loss between the true versus model-infered central BPW is used as the cost function. ADAM optimization (α=0.9, β=0.999) is used with initial learning rate of 0.0002.

6.2.3 Evaluation

The proposed sqeunce-oriented neural network is evaluated to central BPW inference and compared its efficacy with the existing GTF technique, in terms of RMSE error, using the test dataset constructed in Section 6.2.1. Both approaches are trained and evaluated in three different ways, (i) only with brachial BPW, (ii) only with ankle BPW, and (iii) with both of brachial and ankle BPWs, for comparative studies.

In evaluation two different factors are considered, which are variations of age and healthy level, since these two factors is most influent on morphology of BPW. The age is surrogated with Young's modulus of artery considering the fact that the modulus increase with aging. First, the proposed approach is evaluated for the entire dataset. For all datasets, a range of PAD severity is ranged from 0% to 80% occlusive and a range of Young's modulus of artery is ranged from 80% to 400% in an increment of 20% with respect to nominal value, which corresponds to PWV 4.4-15.8m/s and age from 20s to 70s. Second the proposed approach is evaluated for the datasets of young individuals. For all datasets, a range of PAD severity is still ranged from 0% to 80% occlusive, but the range of Young's modulus of artery is ranged from 80% to 200% in an increment of 20%, which corresponds to PWV 4.4-

8.5m/s and age from 20s to 40s. Third, the proposed approach is evaluated for the datasets of healthy datasets. In this case, a range of Young's modulus of artery is ranged from 80% to 400% in an increment of 20% with respect to nominal value, which corresponds to PWV 4.4-15.8m/s and age from 20s to 70s, and a range of PAD severity is ranged from 0% to 40% occlusive. As a last, the proposed approach is evaluated for the datasets of young and healthy individuals. In this case, a range of PAD severity is ranged from 0% to 40% occlusive and the range of Young's modulus of artery is ranged from 80% to 200% in an increment of 20%, which corresponds to PWV 4.4-8.5m/s and age from 20s to 40s.

Furhtermore, the proposed sequence-oriented neural network is analyzed using the saliency algorithm [75] to interpret the discriminative input features exploited by the proposed neural network. Saliency map is applied to visualize the discriminative features (i.e., regions) in the brachial and ankle arterial BP waveforms which largely contributed to infer central BPW. Then, the physiological relevance of the input features exploited by the proposed neural network in infering central BPW is assessed by comparing these discriminative features and the available clinical knowledge on the relationship between central and distal BPWs.

To derive a robust estimate of central BPW inference, the above evaluation is repeated 16 times and reported the average, first quarter, third quarter, and IQR values RMSE error between real and inferred central BPW.

6.3 Central BPW Inference Efficacy

Figure 6-3 represents the example of the inference result of the proposed approach. The proposed approach boasted robust central BPW inference performance superior to the GTF against wide range of PAD severity and age (Figure 6-4). In Figure 6-4, *bsc*, *yng*, *hth*, *y&hth*, and *all* mean the case using entire dataset, dataset of young individuals, dataset of healthy individuals, dataset of young and healthy individuals, and the average of 4 cases, respectively.

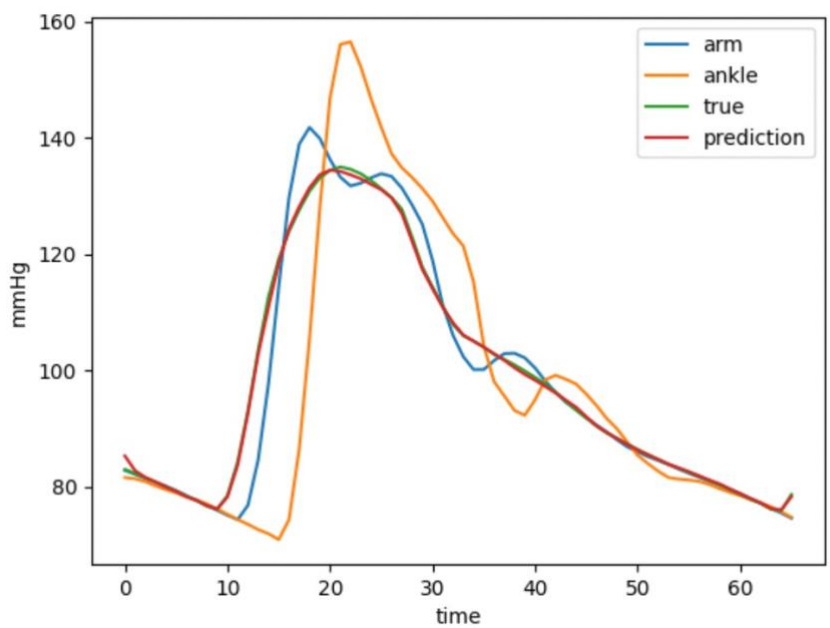

Figure 6-3 An example of the central BPW inference from distal BPWs by the proposed approach.

First, in every case, the inference performance of the proposed approach is superior to the GTF approach with much smaller RMSE values. For the case of when brachial BPW is used only (Figure 6-4 (A) and (D)), the RMSE of the proposed approach is 13%~19% of the RMSE of the GTF approach. For the case of when ankle BPW is used only (Figure 6-4 (B) and (E)), the RMSE of the proposed approach is 18%~24% of the RMSE of the GTF approach. For the case of when both of brachial and ankle BPWs are used (Figure 6-4 (C) and (F)), the RMSE of the proposed approach is 6%~1% of the RMSE of the GTF approach. In this case, it is remarkable that the performance of the proposed approach is enhanced, however the performance of the GTF approach decreases.

Second, for the proposed approach, the performance increases if the dataset is restricted to healthy individuals, and decreases if the dataset is restricted to young individuals. The reason of increased performance with healthy individuals is that the domain that the neural network should be learn become narrow, so that the model is ablt to more fit in. However, the decresed performance with young individuals is not explained with the narrowed domain. It is understanded by the lack of the number of individuals that the model encounters during training. For the GTF approach, both of the case when the dataset of young individuals and the case when the dataset of healthy individuals shows the improved performance with narrowed domain. Since the GTF approach does not requires a large number of individual data, the problem of the lack of the number of individuals does not occur.

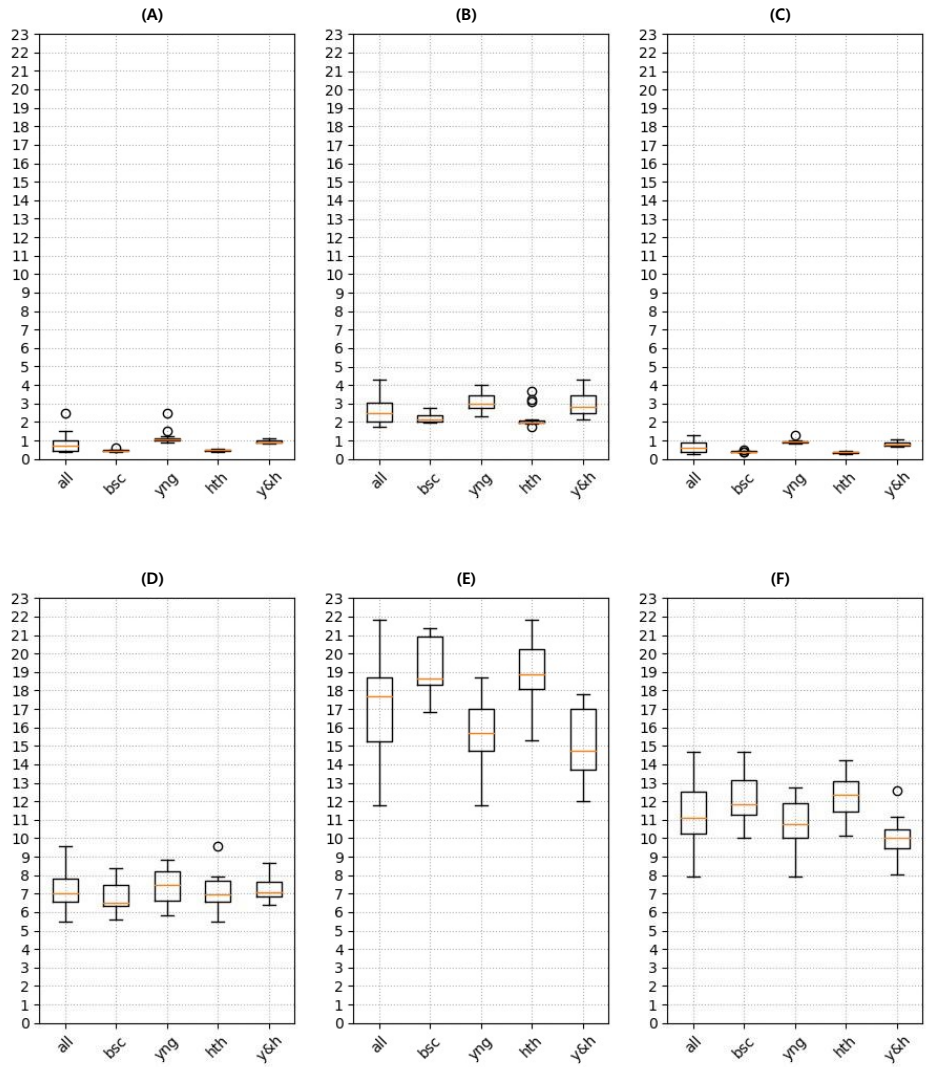

Figure 6-4 RMSE error between real and inferred central BPW. (A) The proposed approach with brachial BPW. (B) The proposed approach with ankle BPW. (C) The proposed approach with both BPWs. (D) The GTF approach with brachial BPW. (E) The GTF approach with ankle BPW. (F) The GTF approach with both BPWs.

Third, for the both of the proposed and GTF approaches, the performance is better when brachial BPW is used as input than when ankle BPW is used. It is because that the brachial artery is closer to central artery, and endure less perturbation during propagation from central to brachial artery. In contrast, the ankle artery is far from centray artery and there are various interaction expecially when the blood flow passes stomach area.

6.4 Interpretability Analysis

The discriminative input features localized by saliency map provide support for the transparency of the sequence-oriented neural network constructed in this work. Indeed, main discriminative input features included (i) the systolic up-stroke and (ii) diastolic down-stroke (including secondary peaks when exists) with its causality (Figure 6-5), which are the regions in the brachial and ankle arterial pulses in which salient morphological mainly changes occur as PAD develops and individual characteristics according to the existing clinical literature [37-42].

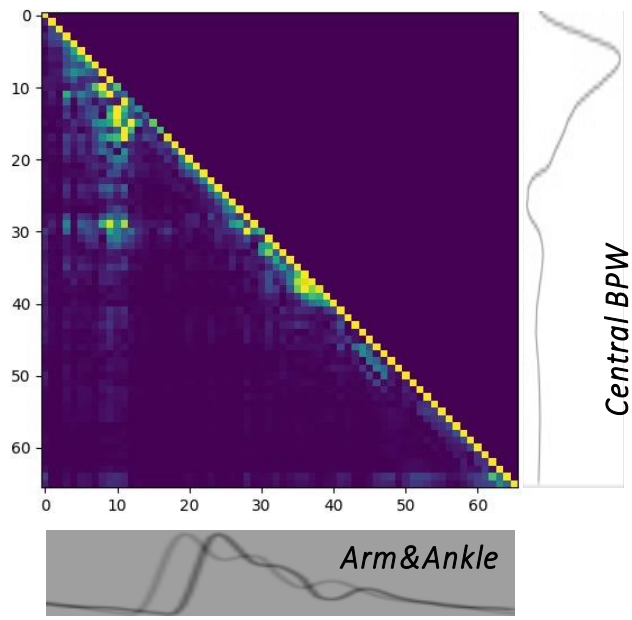

Figure 6-5 An example of saliency map interpretation.

Chapter 7

Conclusions

7.1 Contributions and Significance

This doctoral dissertation aims at advancing three essential and co-related research areas to enable the DNN based arteria disease diagnosis with high accuracy using distal BPW: (1) Research Thrust 1 – a mutually-informed neural network for severity assessment of arterial disease to overcome the sparsity of disease severity levels given in training phase; (2) Research Thrust 2 – a continuous-property adversarial regularization for individuality independency to overcome the sparsity of anatomical and physiological characteristics beyond the training dataset; (3) a sequence-oriented neural network for inference of central BPW to gather the central BPW accurately with non-expensive way.

Contribution 1: A Novel DL Based PWA for PAD Diagnosis Only with BPW datasets under Sparsely Distributed Disease Severity Levels

This doctoral dissertation fundamentally demonstrates the proof-of-concept of a novel DL-based PWA approach to PAD diagnosis. The proposed DL-based PWA is evaluated with virtual patient dataset. The latent space of the proposed DL is

analyzed, and the interpretability analysis is conducted via localization of discriminative input. In advance, A novel method for training DL based PWA model only with the dataset under sparsely distributed disease severity levels is proposed with mutualy-informed neural network.

The unique contributions of this study are two-fold. First, it is a pioneer work to propose a DL based PWA approach to PAD diagnosis, simultaneously suggesting the transparency of neural network by explainable ways. Second, a mutualy-informed neural network enables the high accuracy of PAD diagnosis only with the task-wisely sparsely distributed dataset, which in this case is PAD severity.

Contribution 2: Regularization for Variation of Continuous Anatomical and Physiological Characteristics To Generalize The Diagnosis Model

This doctoral dissertation proposes a continuous-property adversarial regularization to generalize the diagnosis model overcoming the sparsity of anatomical and physiological characteristics. The proposed CPAR is evaluated with virtual patient dataset. The efficacy of CPAR is discussed for the detection and severity assessment performance, and the coverage of CPAR is studied with single/multiple CPAR.

The unique contributions of this study are two-fold. First, the theoretical and empirical penalty term for generalization with respect to continuously variable property is designed. Second, the multiple usage of CPAR for anatomical and physiological characteristic properties enables the high accuracy of PAD diagnosis

overcoming the individual differences.

Contribution 3: Waveform Modulation via Sequential and Feasible DL based Model To Infer Central BPW from Distal BPW

This doctoral dissertation proposes a sequence-oriented neural network to infer the central BPW, which requires excessive cost for acquisition, from distal BPW, which requires much less cost for acquisiton. The proposed sequence-oriented neural network is evaluated with virtual patient datset. The efficacy of the sequence-oriented neural network is discussed with the various case of different characteristics of dataset.

The unique contribution of this study is that the novel architecture of neural network is designed to enables the sequential processing with feasible computational cost. The architecture is independent from given data length and expandable for other types of waveform data, such as electrocardiogram and electroencephalogram.

7.2 Suggestions for Future Research

Although the technical advances proposed in this doctoral dissertation successfully address some issues in the field of arterial disease diagnosis via PWA, there are still several research topics that further investigations and developments are required. Specific suggestions for future research are listed as follows.

Suggestion 1: To Leaverage The Approaches for Data Scarcity by Combining Proposed Thrusts

The thesises were proposed the methods to overcome the scarcity of dataset, especially focusing on the scarcity of severity level in Thrust 1, and the scarcity of individuality in Thrust 2. Both thrusts are heading to identical goal that how to build advanced diagnosis method of arterial disease, but they adopt contrasting directions. In Thrust 1, the scarcity is supplemented by generating virtual data. On the other hand, the scarcity is bypassed in Thrust 2, to make the diagnosis model overlook the effects of parameters which results in scarcity. In reality, the both scarcities exist simultaneously so that they should be considered together. However, there is expected challenges to simply merge both Thrust; the multiplication of both scarcities results in the insufficient dataset to build up a deep learning based diagnosis model. Thus, an advanced method to merge both method with more severe scarcity of dataset is required.

Suggestion 2: To Apply and Validate The Proposed Thesis To Real Patient Data

The thesises were conducted using data collected from virtual rather than real patients. A validated multi-branch TL model was employed to create virtual patients. It is also shown that arterial pulse waveforms produced by the virtual patients exhibit the morphological characteristics observed in real PAD patients. Yet, discrepancy between virtual versus real patients may be inevitable at least to some extent, and there are a few potential sources that can obscure the initial success of this work when applied to real clinical data. In particular, the inter- and intra-individual variability considered in this work is somewhat ad-hoc. Furthermore, variability is accounted for associated only with arterial anatomical and physiological parameters but not cardiac parameters (such as stroke volume and ejection duration). In the near term, the efficacy of the proposed approach against variabilities not considered in this work may be investigated using the same virtual patients. But ultimately, future work must confirm the proof-of-concept obtained in this work using clinical data collected from real patients.

Suggestion 3: To Expand The Coverage of Disease Diagnosis

In this dissertation, PAD was mainly concerned as a representative example. PAD is leading portion of arterial disease, and it is one of the most important arterial disease that should be monitored closely. Neverthlese, there are other arterial diseases that show crucial mortality, such as aneurysm and/or an arterial stiffening. Aneurysm is an occurrence of ballon-like bulge in artery which could be dissect or rupture, and arterial stiffening is a generalized thickening and stiffening of the arterial wall which results in high blood pressure or hyper-tension. Since these

arterial disease also highly related with blood pressure of artery interacting the morphology of BPW, the extension of the coverage of the dissertation's topic could be followed.

Suggestion 4: To Utilize The Additional Biometric Data

The blood pressure waveform is one of the most important biometric data and the pulse waveform analysis is conducted on BPW since it could yield useful diagnosis result related with cardiovascular health status. Meanwhile, there are other biometric waveform data such as electrocardiogram and electroencephalogram, and the researches that analyze such electromagnetic waveform data have been also widely conducted. The thesises of this dissertations were proposed to BPW analysis, but also it has a opportunity to extended to other biometric waveform data since they also share similar challenges that this dissertation focused on.

References

[1] M. A. Allison *et al.*, "Ethnic-specific prevalence of peripheral arterial disease in the United States," *American journal of preventive medicine,* vol. 32, no. 4, pp. 328-333, 2007.

[2] H. Yu *et al.*, "Human infection with avian influenza A H7N9 virus: an assessment of clinical severity," *The Lancet,* vol. 382, no. 9887, pp. 138-145, 2013.

[3] F. G. R. Fowkes *et al.*, "Comparison of global estimates of prevalence and risk factors for peripheral artery disease in 2000 and 2010: a systematic review and analysis," *The lancet,* vol. 382, no. 9901, pp. 1329-1340, 2013.

[4] B. A. Golomb, T. T. Dang, and M. H. Criqui, "Peripheral arterial disease: morbidity and mortality implications," *Circulation,* vol. 114, no. 7, pp. 688-699, 2006.

[5] A. Hirsch, "Criqui MH, Treat-Jacobson D, Regensteiner JG, Creager MD, Olin JW, Krook SH, Hunningshake DM, Comerota AJ, Walsh WE, McDermott MM, and Hiatt WR," *Peripheral arterial disease detection, awareness, and treatment in primary care. JAMA,* vol. 286, pp. 1317-1324, 2001.

[6] A. T. Hirsch *et al.*, "Peripheral arterial disease detection, awareness, and treatment in primary care," *Jama,* vol. 286, no. 11, pp. 1317-1324, 2001.

[7] A. U. Cavallo *et al.*, "Noncontrast magnetic resonance angiography for the diagnosis of peripheral vascular disease," *Circulation: Cardiovascular Imaging,* vol. 12, no. 5, p. e008844, 2019.

[8] D. F. Guthaner *et al.*, "Evaluation of peripheral vascular disease using digital subtraction angiography," *Radiology,* vol. 147, no. 2, pp. 393-398, 1983.

[9] M. Romano *et al.*, "Multidetector row CT angiography of the abdominal aorta and lower extremities in patients with peripheral arterial occlusive disease: diagnostic accuracy and interobserver agreement," *European journal of radiology,* vol. 50, no. 3, pp. 303-308, 2004.

[10] M. R. Nelson, S. Quinn, T. M. Winzenberg, F. Howes, L. Shiel, and C. M. Reid, "Ankle-Brachial Index determination and peripheral arterial disease diagnosis by an oscillometric blood pressure device in primary care: validation and diagnostic accuracy study," *BMJ open,* vol. 2, no. 5, p. e001689, 2012.

[11] M. Abdar, W. Książek, U. R. Acharya, R.-S. Tan, V. Makarenkov, and P. Pławiak, "A new machine learning technique for an accurate diagnosis of coronary artery disease," *Computer methods and programs in biomedicine,* vol. 179, p. 104992, 2019.

[12] M. V. Dogan, I. M. Grumbach, J. J. Michaelson, and R. A. Philibert, "Integrated genetic and epigenetic prediction of coronary heart disease in the Framingham Heart Study," *PloS one,* vol. 13, no. 1, p. e0190549, 2018.

[13] A. Vallée, A. Cinaud, V. Blachier, H. Lelong, M. E. Safar, and J. Blacher,

"Coronary heart disease diagnosis by artificial neural networks including aortic pulse wave velocity index and clinical parameters," *Journal of hypertension,* vol. 37, no. 8, pp. 1682-1688, 2019.

[14] A. M. Alaa, T. Bolton, E. Di Angelantonio, J. H. Rudd, and M. van der Schaar, "Cardiovascular disease risk prediction using automated machine learning: a prospective study of 423,604 UK Biobank participants," *PloS one,* vol. 14, no. 5, p. e0213653, 2019.

[15] B. Ambale-Venkatesh *et al.*, "Cardiovascular event prediction by machine learning: the multi-ethnic study of atherosclerosis," *Circulation research,* vol. 121, no. 9, pp. 1092-1101, 2017.

[16] A. J. Steele, S. C. Denaxas, A. D. Shah, H. Hemingway, and N. M. Luscombe, "Machine learning models in electronic health records can outperform conventional survival models for predicting patient mortality in coronary artery disease," *PloS one,* vol. 13, no. 8, p. e0202344, 2018.

[17] A. Abdolmanafi, L. Duong, N. Dahdah, I. R. Adib, and F. Cheriet, "Characterization of coronary artery pathological formations from OCT imaging using deep learning," *Biomedical optics express,* vol. 9, no. 10, pp. 4936-4960, 2018.

[18] R. Poplin *et al.*, "Prediction of cardiovascular risk factors from retinal fundus photographs via deep learning," *Nature Biomedical Engineering,* vol. 2, no. 3, pp. 158-164, 2018.

[19] N. Zhang *et al.*, "Deep learning for diagnosis of chronic myocardial infarction on nonenhanced cardiac cine MRI," *Radiology,* vol. 291, no. 3, pp. 606-617, 2019.

[20] A. M. Arruda-Olson *et al.*, "Leveraging the electronic health record to create an automated real-time prognostic tool for peripheral arterial disease," *Journal of the American Heart Association,* vol. 7, no. 23, p. e009680, 2018.

[21] E. G. Ross, N. H. Shah, R. L. Dalman, K. T. Nead, J. P. Cooke, and N. J. Leeper, "The use of machine learning for the identification of peripheral artery disease and future mortality risk," *Journal of vascular surgery,* vol. 64, no. 5, pp. 1515-1522. e3, 2016.

[22] S. Gol, R. N. Pena, M. F. Rothschild, M. Tor, and J. Estany, "A polymorphism in the fatty acid desaturase-2 gene is associated with the arachidonic acid metabolism in pigs," *Scientific reports,* vol. 8, no. 1, pp. 1-9, 2018.

[23] S. E. Nejad, J. P. Carey, M. S. McMurtry, and J.-O. Hahn, "Model-based cardiovascular disease diagnosis: a preliminary in-silico study," *Biomechanics and modeling in mechanobiology,* vol. 16, no. 2, pp. 549-560, 2017.

[24] H. Xiao, A. Avolio, and D. Huang, "A novel method of artery stenosis diagnosis using transfer function and support vector machine based on transmission line model: A numerical simulation and validation study," *Computer methods and programs in biomedicine,* vol. 129, pp. 71-81, 2016.

[25] S. Kim, J.-O. Hahn, and B. D. Youn, "Detection and Severity Assessment of Peripheral Occlusive Artery Disease via Deep Learning Analysis of Arterial Pulse Waveforms: Proof-of-Concept and Potential Challenges," *Frontiers in Bioengineering and Biotechnology,* vol. 8, p. 720, 2020.

[26] Z. Ghasemi *et al.*, "Estimation of cardiovascular risk predictors from non-invasively measured diametric pulse volume waveforms via multiple measurement information fusion," *Scientific reports,* vol. 8, no. 1, p. 10433, 2018.

[27] G. Li, K. Watanabe, H. Anzai, X. Song, A. Qiao, and M. Ohta, "Pulse-wave-pattern classification with a convolutional neural network," *Scientific reports,* vol. 9, no. 1, pp. 1-11, 2019.

[28] R. Mukkamala *et al.*, "Toward ubiquitous blood pressure monitoring via pulse transit time: theory and practice," *IEEE Transactions on Biomedical Engineering,* vol. 62, no. 8, pp. 1879-1901, 2015.

[29] E. Agabiti-Rosei *et al.*, "Central blood pressure measurements and antihypertensive therapy: a consensus document," *Hypertension,* vol. 50, no. 1, pp. 154-160, 2007.

[30] C. Wang *et al.*, "Monitoring of the central blood pressure waveform via a conformal ultrasonic device," *Nature biomedical engineering,* vol. 2, no. 9, pp. 687-695, 2018.

[31] Y. Ganin *et al.*, "Domain-adversarial training of neural networks," *The Journal of Machine Learning Research,* vol. 17, no. 1, pp. 2096-2030, 2016.

[32] A. v. d. Oord *et al.*, "Wavenet: A generative model for raw audio," *arXiv preprint arXiv:1609.03499,* 2016.

[33] W. He, H. Xiao, and X. Liu, "Numerical simulation of human systemic arterial hemodynamics based on a transmission line model and recursive algorithm," *Journal of Mechanics in Medicine and Biology,* vol. 12, no. 01, p. 1250020, 2012.

[34] J. Womersley, "Oscillatory flow in arteries: the constrained elastic tube as a model of arterial flow and pulse transmission," *Physics in Medicine & Biology,* vol. 2, no. 2, p. 178, 1957.

[35] H. Xiao, A. Avolio, and M. Zhao, "Modeling and hemodynamic simulation of human arterial stenosis via transmission line model," *Journal of Mechanics in Medicine and Biology,* vol. 16, no. 05, p. 1650067, 2016.

[36] H. Xiao, I. Tan, M. Butlin, D. Li, and A. P. Avolio, "Arterial viscoelasticity: role in the dependency of pulse wave velocity on heart rate in conduit arteries," *American Journal of Physiology-Heart and Circulatory Physiology,* vol. 312, no. 6, pp. H1185-H1194, 2017.

[37] S. Carter, "Clinical measurements of systolic pressure in limbs with arterial occlusive disease in the lower extremities," *Circulation,* vol. 38, pp. 624-637, 1968.

[38] J. H. Davies, J. E. Lewis, and E. M. Williams, "The utility of pulse volume waveforms in the identification of lower limb arterial insufficiency," 2014.

[39] D. Dhanoa *et al.*, "Position statement on noninvasive imaging of peripheral arterial disease by the Society of Interventional Radiology and the Canadian Interventional Radiology Association," *J Vasc Interv Radiol,* vol. 27, no. 7, pp. 947-51, 2016.

[40] Y. Mao *et al.*, "Incidence of peripheral arterial disease and its association with pulse pressure: a prospective cohort study," *Frontiers in endocrinology,* vol. 8, p. 333, 2017.

[41] R. C. Sibley III, S. P. Reis, J. J. MacFarlane, M. A. Reddick, S. P. Kalva, and P. D. Sutphin, "Noninvasive physiologic vascular studies: A guide to diagnosing peripheral arterial disease," *Radiographics,* vol. 37, no. 1, pp. 346-357, 2017.

[42] E. Benitez and B. E. Sumpio, "Pulse volume recording for peripheral vascular disease diagnosis in diabetes patients," *Journal of Vascular Diagnostics and Interventions,* vol. 3, p. 33, 2015.

[43] A. Krizhevsky, I. Sutskever, and G. E. Hinton, "Imagenet classification with deep convolutional neural networks," *Advances in neural information processing systems,* vol. 25, pp. 1097-1105, 2012.

[44] K. He, X. Zhang, S. Ren, and J. Sun, "Identity mappings in deep residual networks," in *European conference on computer vision*, 2016: Springer, pp. 630-645.

[45] G. Huang, Z. Liu, L. Van Der Maaten, and K. Q. Weinberger, "Densely Connected Convolutional Networks," in *CVPR*, 2017, vol. 1, no. 2, p. 3.

[46] R. R. Selvaraju, M. Cogswell, A. Das, R. Vedantam, D. Parikh, and D. Batra, "Grad-cam: Visual explanations from deep networks via gradient-based localization," in *Proceedings of the IEEE International Conference on Computer Vision*, 2017, pp. 618-626.

[47] R. Stein, I. Hriljac, J. L. Halperin, S. M. Gustavson, V. Teodorescu, and J. W. Olin, "Limitation of the resting ankle-brachial index in symptomatic patients with peripheral arterial disease," *Vascular medicine,* vol. 11, no. 1, pp. 29-33, 2006.

[48] J. Wikström, T. Hansen, L. Johansson, L. Lind, and H. Ahlström, "Ankle brachial index< 0.9 underestimates the prevalence of peripheral artery occlusive disease assessed with whole-body magnetic resonance angiography in the elderly," *Acta radiologica,* vol. 49, no. 2, pp. 143-149, 2008.

[49] J. Lee *et al.*, "Investigation of viscoelasticity in the relationship between carotid artery blood pressure and distal pulse volume waveforms," *IEEE journal of Biomedical and Health Informatics,* vol. 22, no. 2, pp. 460-470, 2017.

[50] L. Brillouin, *Science and information theory*. Courier Corporation, 2013.

[51] I. Goodfellow *et al.*, "Generative adversarial nets," in *Advances in neural information processing systems*, 2014, pp. 2672-2680.

[52] C. K. Sønderby, J. Caballero, L. Theis, W. Shi, and F. Huszár, "Amortised

map inference for image super-resolution," *arXiv preprint arXiv:1610.04490,* 2016.

[53] K. Bousmalis, N. Silberman, D. Dohan, D. Erhan, and D. Krishnan, "Unsupervised pixel-level domain adaptation with generative adversarial networks," in *Proceedings of the IEEE conference on computer vision and pattern recognition*, 2017, pp. 3722-3731.

[54] Y. Choi, M. Choi, M. Kim, J.-W. Ha, S. Kim, and J. Choo, "Stargan: Unified generative adversarial networks for multi-domain image-to-image translation," *arXiv preprint,* vol. 1711, 2017.

[55] S. Pascual, A. Bonafonte, and J. Serrà, "SEGAN: Speech enhancement generative adversarial network," *arXiv preprint arXiv:1703.09452,* 2017.

[56] X. Chen, Y. Duan, R. Houthooft, J. Schulman, I. Sutskever, and P. Abbeel, "Infogan: Interpretable representation learning by information maximizing generative adversarial nets," in *Advances in neural information processing systems*, 2016, pp. 2172-2180.

[57] M. Huh, P. Agrawal, and A. A. Efros, "What makes ImageNet good for transfer learning?," *arXiv preprint arXiv:1608.08614,* 2016.

[58] S. J. Pan and Q. Yang, "A survey on transfer learning," *IEEE Transactions on knowledge and data engineering,* vol. 22, no. 10, pp. 1345-1359, 2009.

[59] M. Ghafoorian *et al.*, "Transfer learning for domain adaptation in mri: Application in brain lesion segmentation," in *International conference on medical image computing and computer-assisted intervention*, 2017: Springer, pp. 516-524.

[60] G. Liang and L. Zheng, "A transfer learning method with deep residual network for pediatric pneumonia diagnosis," *Computer methods and programs in biomedicine,* vol. 187, p. 104964, 2020.

[61] R. K. Samala, H.-P. Chan, L. Hadjiiski, M. A. Helvie, C. D. Richter, and K. H. Cha, "Breast cancer diagnosis in digital breast tomosynthesis: effects of training sample size on multi-stage transfer learning using deep neural nets," *IEEE transactions on medical imaging,* vol. 38, no. 3, pp. 686-696, 2018.

[62] F. Girosi, M. Jones, and T. Poggio, "Regularization theory and neural networks architectures," *Neural computation,* vol. 7, no. 2, pp. 219-269, 1995.

[63] H. Li, S. J. Pan, S. Wang, and A. C. Kot, "Domain generalization with adversarial feature learning," in *Proceedings of the IEEE Conference on Computer Vision and Pattern Recognition*, 2018, pp. 5400-5409.

[64] D. Wu, S.-T. Xia, and Y. Wang, "Adversarial weight perturbation helps robust generalization," *arXiv preprint arXiv:2004.05884,* 2020.

[65] T. Han, Y.-F. Li, and M. Qian, "A hybrid generalization network for intelligent fault diagnosis of rotating machinery under unseen working conditions," *IEEE Transactions on Instrumentation and Measurement,* 2021.

[66] Y. Zhang and Q. Yang, "A survey on multi-task learning," *arXiv preprint arXiv:1707.08114,* 2017.

[67] S. Ben-David, J. Blitzer, K. Crammer, and F. Pereira, "Analysis of representations for domain adaptation," *Advances in neural information processing systems,* vol. 19, p. 137, 2007.
[68] S. Ben-David, J. Blitzer, K. Crammer, A. Kulesza, F. Pereira, and J. W. Vaughan, "A theory of learning from different domains," *Machine learning,* vol. 79, no. 1, pp. 151-175, 2010.
[69] M. Gao, W. C. Rose, B. Fetics, D. A. Kass, C.-H. Chen, and R. J. S. r. Mukkamala, "A simple adaptive transfer function for deriving the central blood pressure waveform from a radial blood pressure waveform," vol. 6, p. 33230, 2016.
[70] L. Ljung, "Theory for the User," *System Identification,* 1987.
[71] C.-H. Chen *et al.*, "Estimation of central aortic pressure waveform by mathematical transformation of radial tonometry pressure: validation of generalized transfer function," *Circulation,* vol. 95, no. 7, pp. 1827-1836, 1997.
[72] N. Fazeli *et al.*, "Subject-specific estimation of central aortic blood pressure via system identification: preliminary in-human experimental study," *Medical & biological engineering & computing,* vol. 52, no. 10, pp. 895-904, 2014.
[73] K. He, X. Zhang, S. Ren, and J. Sun, "Deep residual learning for image recognition," in *Proceedings of the IEEE conference on computer vision and pattern recognition*, 2016, pp. 770-778.
[74] S. Hochreiter and J. Schmidhuber, "Long short-term memory," *Neural computation,* vol. 9, no. 8, pp. 1735-1780, 1997.
[75] S. Hong, T. You, S. Kwak, and B. Han, "Online tracking by learning discriminative saliency map with convolutional neural network," in *International conference on machine learning*, 2015: PMLR, pp. 597-606.

국문 초록

개인 편차에 대해 정규화되고 설명 가능한 인공지능 기반 중심혈압파형 추론 및 심혈관계 질환 진단 방법 연구

동맥질환은 대표적인 심혈관계 질환으로 말초동맥폐쇄질환, 대동맥류, 동맥경화 등이 있으며, 이는 전세계적으로 가장 높은 사망 원인 중 하나이다. 동맥질환은 질환발병률 및 사망률이 높고 전세계적으로 널리 퍼져있으며, 특히 사회가 고령화되면서 급격히 증가할 것으로 예측되고 있다. 임상적으로 동맥질환 진단에는 혈관 조영 기술이 사용되나, 이는 높은 비용의 비일상적인 측정을 수반하여 지속적인 동맥 질환 감지 및 질환 심각도 진단에 적합하지 않다.

동맥 펄스 파형 분석은 기계학습 기술의 접목을 통해 동맥질환 진단에 활용될 수 있다. 동맥질환은 동맥 맥파 전파 및 반사특성에 영향을 미침으로써 혈압파형의 형태를 변화시킨다. 따라서 혈압파형의 형태를 분석하여 동맥질환을 진단하는 것이 기존의 기술을 능가할 가능성이 있다. 또한 동맥 펄스 파형 분석은 최근 급격히 진보된 딥러닝 기술과 결합하여 자율적인 특성인자 추출을 통한 진단 성능을 향상시킬 수 있을 것으로 기대된다. 한편, 동맥 펄스 파형 분석에 대한 임상적인 접근 방식으로는 신체 중심부에서 획득된 혈압 파형데이터가 더욱 주목된다. 중심 혈압 파형은 동적인 심혈관계 상태에 대한 다양한 정보를 제공할 수 있다는 점에서 그 가치가 부각된다.

이러한 동맥 펄스 파형 분석 기반 심혈관계 질환 진단 기술에 인공지능 기술을 결합하는 것에는 세가지 치명적인 문제가 존재한다. 첫째로, 동맥 혈압 파형 데이터가 제한적이다. 인공지능 기술을 동맥 펄스 파형 분석 기반 심혈관계 질환 진단에 활용하기 위해서는 시간에 따라 질환이 발전되는 다량의 동적인 데이터가 필요하다. 뿐만 아니라, 환자는 다양한 해부학적 및 생리학적 특징을 갖고 있으며 따라서 다양한 환자들로부터 축적된 데이터가 필요하다. 하지만 임상적으로는 (1) 오직

제한된 질환 심각도의 환자로부터 획득된 데이터만 획득가능하며 주로 질환초기 및 질환이 존재하지 않는 환자 혹은 질환이 상당수준 진행된 환자의 데이터만이 획득 가능하다. 또한 (2) 제한된 수의 환자로부터 획득된 데이터만이 확보 가능하며, 다양한 해부학적 및 생리학적 특징을 포과할 수 없다. 한편 이러한 편차로부터 비교적 독립적인 중심혈압파형 분석에는 (3) 데이터 획득에 높은수준의 비용이 발생하며, 도뇨관 설치와 같은 침습적인 방법으로만 획득 가능하다.

이에 본 박사학위논문에서는 (1) 희박하게 분포된 질환 심각도의 데이터 한계를 극복하기 위한 상호 정보기반 인공지능 기술 연구, (2) 다양한 개인의 편차로 인한 진단 정확도의 하락을 극복하기 위한 연속변수적대적 정규화 기술 연구, (3) 비침습적 데이터를 활용하여 중심 혈압 파형을 추론하기 위한 시퀀스 지향적 신경망 기술 연구를 제안한다.

첫번째 연구에서는 딥러닝 기반 동맥 펄스 파형 분석의 초기 증명을 제시하고, 실제 임상 적용을 위해 해결되어야하는 과제 및 방향성을 제시한다. 본 연구에서는 예비 연구로서 상완 및 발목 동맥 혈압파형 분석에 기반하여 질환 심각도를 감지 및 평가할 수 있는 합성곱 신멱망을 구성하고, 딥러닝 기반 기술의 효과를 증명하기 위해 발목-상완지수(ABI)와의 성능 비교 및 딥러닝의 잠재 특성인자 공간 분석을 통한 시각화 결과가 제시된다. 또한 상호정보를 사용하여 희소한 질환 심각도에서의 데이터만을 사용하여 딥러닝 기반 질환 진단모델을 교육하는 방법이 제시된다. 이를 위해 가상 데이터 생성모델과 질환 진단 모델이 함께 학습되며, 질환 심각도와 잠재 특성인자, 혈압 파형 데이터간의 상호 정보를 극대화하여 진단 모델의 성능을 향상시킨다.

두번째 연구에서는 해부학적 및 생리학적 특성에 대해 딥러닝 기반 진단 모델의 일반화를 위한 연속변수적대적 정규화(Continuous-Property-Adversarial Regularization) 기술을 제시한다. 본 연구에서는 도메인 적대적 학습에 기반하여 기존의 이산 도메인 적대적 정규화 및 도메인 일반화 기술을 연속된 도메인에 대한 적대적 학습으로 확장한다. 이를 위해 도메인 특성은 연속된 변수의 함수로 표현되며, 여러 연속 변수에 대한 적대적 학습을 통해 제안된 기술은 도메인 변화에 독립적인 잠재 특성인자를 추출하고, 최종적으로 개인 편차에 독립하여 질환을 진단한다.

세번째 연구에서는 원위 혈압파형을 변조하여 중심 혈압파형을 추론하는 시퀀스 지향 신경망 기술을 제시한다. 본 연구에서는 파형 데이터 변조를 위해 상대적으로 계산 비용이 낮은 합성곱 신경망 기반 모델을 사용하면서도 데이터의 순차적 특성을 보존하도록 설계하여 중심혈압파형의 정확한 추론을 가능하게 한다. 이를 위해 시퀀스 지향

신경망은 단측 레이어, 마스킹 레이어, 버틀넥 레이어로 구성된 합성곱 신경망 기반 시퀀스 지향 부 신경망을 구축하고, 이를 재귀적 신경망에 연결하여 최종 중심 혈압 파형을 추론한다.

주요어: 동맥 질환 진단
말초 동맥 질환
동맥 펄스 분석
혈압 파형
심층 신경망

학 번: 2017-28145